Photoactive [2]Rotaxanes: Structure and Photophysical Properties of Anthracene- and Ferrocene-Stoppered [2]Rotaxanes

Andrew C. Benniston,[†] Anthony Harriman,*[,†] and Vincent M. Lynch[‡]

Contribution from the Center for Fast Kinetics Research and Department of Chemistry and Biochemistry, University of Texas at Austin, Austin, Texas 78712

Received September 8, 1994[⊗]

Abstract: The structures of several one- and two-station [2]rotaxanes have been probed in both solid and solution phases. It is shown that the cyclophane, comprising two 4,4′-bipyridinium dications linked *via* 1,4-xylyl groups, resides preferentially over a dialkoxybenzene subunit incorporated into the "string". The terminal stoppers, anthracene or ferrocene subunits, associate with the exterior of the cyclophane, *via* π-stacking, so as to form closed conformations. Excitation into the anthracene stoppers is followed by rapid, but reversible, electron transfer to the cyclophane. Direct excitation into the charge-transfer absorption band results in formation of an intimate radical ion pair in which an electron has been transferred from the central dialkoxybenzene donor to the cyclophane acceptor. Rapid charge recombination occurs but can be partially intercepted by hole transfer to an appended ferrocene stopper. In this latter case, the ground state is restored by relatively slow electron transfer from the reduced cyclophane to the terminal ferrocenium cation. It is proposed that the closed conformation unwinds subsequent to this second electron-transfer step in order to minimize electrostatic repulsion. To some extent, therefore, the rates of electron transfer are controlled by conformational exchange.

The recent emergence of supramolecular chemistry[1] has led to the possibility of constructing large arrays which contain either redox- or photoactive groups in well-defined and logically-sited spatial arrangements.[2] In particular, the use of noncovalent bonding to optimally position molecules so as to facilitate rapid and unidirectional electron-transfer processes has received much attention.[3–6] One particularly attractive means of interlocking adjacent molecular modules into a larger structure involves exploiting the associative interaction that occurs upon contact between an electron donor and a complementary electron acceptor.[7] Indeed, the close proximity of such molecular subunits can result in formation of a complex that exhibits a pronounced charge-transfer absorption transition in the visible region of the spectrum.[8] Illumination into this absorption band results in the generation of an intimate radical ion pair (RIP) due to facile electron transfer from donor to acceptor. This is an extremely simple method for producing a charge-separated state, but it is often found that ultrafast charge recombination restores the ground-state system[9] before solvent penetration and diffusive separation can provide for formation of solvated radical ions. A further disadvantage of such complexes, as regards devising useful molecular devices, concerns their very low binding constants (e.g., $<1\ M^{-1}$). This particular problem can be overcome by constraining either donor or acceptor into a cyclophane that can bind its complementary partner within its central cavity,[10] allowing for discrimination by virtue of size, shape, and redox power. Using this approach, especially with cyclophanes formed by cyclizing two electron-deficient 4,4′-bipyridinium dication subunits,[11] a number of multicomponent molecular arrays have been synthesized.[12]

Recent studies[10,13] have shown that numerous electron donors can be included into the central cavity of the above cyclophane; this is a particularly versatile and avid receptor that has many promising applications.[14] The resultant complexes, for which association constants typically lie within the range $10–200\ M^{-1}$, exhibit a strong charge-transfer absorption band in the visible spectral region. It has been shown, however, that the RIP produced upon excitation into this charge-transfer absorption band with a short laser pulse undergoes very fast charge recombination, and only in certain cases was there dissociation of the RIP.[10] In order to extend the lifetime of the RIP it proved necessary to attach a second electron donor[15] (or acceptor)[16] to

[†] Center for Fast Kinetics Research.

[‡] Department of Chemistry and Biochemistry.

[⊗] Abstract published in *Advance ACS Abstracts,* May 1, 1995.

(1) Lehn, J.-M. *Angew. Chem., Int. Ed. Engl.* **1988**, *27*, 89.

(2) Balzani, V.; Scandola, F. *Supramolecular Photochemistry*; Horwood: Chichester, 1991.

(3) Vögtle, F.; Müller, W. M.; Müller, T.; Bauer, M.; Rissanen, K. *Angew. Chem., Int. Ed. Engl.* **1993**, *32*, 1295.

(4) Segawa, H.; Takehara, C.; Honda, K.; Shimidzu, T.; Asahi, T.; Mataga, N. *J. Phys. Chem.* **1992**, *96*, 503.

(5) Harriman, A.; Odobel, F.; Sauvage, J.-P. *J. Am. Chem. Soc.* **1994**, *116*, 5481.

(6) Sessler, J. L.; Wang, B.; Harriman, A. *J. Am. Chem. Soc.* **1993**, *115*, 10418.

(7) Hastings, S. H.; Franklin, J. L.; Schiller, J. C.; Matsen, F. A. *J. Am. Chem. Soc.* **1953**, *75*, 2900.

(8) Mulliken, R. S. *J. Am. Chem. Soc.* **1952**, *74*, 811.

(9) (a) Asahi, T.; Mataga, N. *J. Phys. Chem.* **1991**, *95*, 1956. (b) Asahi, T.; Ohkohchi, M.; Mataga, N. *J. Phys. Chem.* **1993**, *97*, 13132.

(10) Benniston, A. C.; Harriman, A.; Philp, D.; Stoddart, J. F. *J. Am. Chem. Soc.* **1993**, *115*, 5298.

(11) Odell, B.; Reddington, M. V.; Slawin, A. M. Z.; Spencer, N.; Stoddart, J. F.; Williams, D. *Angew. Chem., Int. Ed. Engl.* **1988**, *11*, 1547.

(12) See, for example: (a) Ashton, P. R.; Reder, A. S.; Spencer, N.; Stoddart, J. F. *J. Am. Chem. Soc.* **1993**, *115*, 5286. (b) Amabilino, D. B.; Ashton, P. R.; Reder, A. S.; Spencer, N.; Stoddart, J. F. *Angew. Chem., Int. Ed. Engl.* **1994**, *33*, 1286. (b) Bissell, R. A.; Cordova, E.; Kaifer, A. E.; Stoddart, J. F. *Nature* **1994**, *369*, 133. (c) Gunter, M. J.; Hockless, D. C. R.; Johnson, M. R.; Skelton, B. W.; White, A. H. *J. Am. Chem. Soc.* **1994**, *116*, 4810. (d) Ashton, P. R.; Brown, C. L.; Chrystal, E. J. T.; Parry, K. P.; Pietraszkiewicz, M.; Spencer, N.; Stoddart, J. F. *Angew. Chem., Int. Ed. Engl.* **1991**, *30*, 1042.

(13) Bernado, A. R.; Stoddart, J. F.; Kaifer, A. E. *J. Am. Chem. Soc.* **1992**, *114*, 10624.

(14) See for example: (a) Leutwyler, K. *Sci. Am.* **1994**, August issue, 87. (b) Dagani, R. *Chem. Eng. News* **1994**, *11*, 1547.

(15) Benniston, A. C.; Harriman, A. *Angew. Chem., Int. Ed. Engl.* **1993**, *32*, 1459.

0002-7863/95/1517-5275$09.00/0

the supramolecular system in such a way as to facilitate sequential electron transfer, leading to spatial separation of the redox equivalents. A simple means of constructing such complex arrays is *via* formation of [2]rotaxanes whereby redox-active groups are attached at the end of a flexible "string" which passes through the cyclophane.[15,17] Of course, the redox-active groups must be sufficiently bulky so as to prevent dissociation of the [2]rotaxane.

The rapid rate of charge recombination observed in the unstopperred cyclophane-derived complexes[10] demands that electron transfer to the terminal donor must also be fast if this process is to be competitive. This, in turn, means that there must be some level of preorganization within the [2]rotaxane that positions the secondary donor close to the charge-transfer complex prior to excitation. In this report, we demonstrate that this requisite can be accommodated *via* π-stacking between cyclophane and terminal donor.[17] It is further proposed that laser activation of such supramolecular arrays causes coherent migration of the cyclophane along the string, with concomitant unraveling of the conformer.

Experimental Section

General Methods. Raw materials and chemicals used for purification purposes were purchased from Aldrich Chemicals and, unless stated otherwise, were used as received. Acetonitrile (HPLC grade) and dichloromethane (spectroscopic grade) were dried over CaH_2 and redistilled before use, while triethylamine was redistilled from NaOH. 1,4-Bis[2-hydroxyethoxy)ethoxy]ethoxy]benzene **7**,[18] 1,1′-[1,4-phenylenebis(methylene)bis-4,4′-bipyridinium bis(hexafluorophosphate) **6**,[18] and 1,11-bis[2-(2-hydroxyethoxy)ethoxy)ethoxy)phenoxy]-3,6,9-trioxundecane **11**[18] were prepared by literature methods; the latter was prepared by a slight modification of the published method.[19] 9-Anthroyl chloride was prepared from the corresponding carboxylic acid using thionyl chloride.[20] Ethyl and decyl 9-anthroate were prepared[21] by esterification of 9-anthroyl chloride and purified by column chromatography. Ferrocenoyl chloride[22] was prepared from ferrocenecarboxylic acid using oxalyl chloride in dichloromethane. Synthesis of [2]rotaxane **3** has been described previously,[15] and the new [2]rotaxanes **1**, **2**, **4**, and **5** were prepared by a similar method using strings, **8**, **10**, **13**, and **12**, respectively, prepared as described below. Column chromatography was achieved with silica gel (SiliCar grade, 60−200 mesh) obtained from Mallinckrodt. Melting points were obtained with a Mel-temp instrument and were uncorrected.

Synthesis of the Strings. Preparation of 8. 9-Anthroyl chloride (2.0 g, 8.3 mmol) and 1,4-bis[2-[2-(2-hydroxyethoxy)ethoxy]ethoxy]-benzene **7** (1.6 g, 4.3 mmol) were refluxed in dried CH_3CN (50 mL) for 12 h. The solvent was removed under vacuum, and the resultant oil was chromatographed on silica gel eluting first with hexanes, in order to remove unreacted 9-anthroyl chloride, and subsequently with ethyl acetate/hexanes 1:1 to remove the desired product as a yellow oil: yield 1.5 g, 45%; ^{1}H NMR (250 MHz, $CDCl_3$) δ = 3.76−3.81 (m, 12H); 3.93−3.98 (m, 8H); 4.77−4.81 (t, 4H, J = 4.6 Hz); 6.74 (s, 4H); 7.43−7.56 (m, 8H); 7.98−8.01 (d, 4H, J = 7.9 Hz); 8.12−8.15 (d, 4H, J = 7.9 Hz); 8.51 (s, 2H); ^{13}C NMR ($CDCl_3$) δ = 64.54; 67.93; 69.11; 69.93; 70.70; 70.82; 115.45; 125.15; 126.92; 128.50; 129.41; 130.93; 152.97; 169.45; FAB-MS (nitrobenzyl alcohol) m/z = 782 $[M]^+$; calculated for $C_{48}H_{46}O_{10}$ 782.3091, found 782.3101.

Preparation of 9. Ferrocenoyl chloride (0.8 g, 3.2 mmol) in dried CH_2Cl_2 (25 mL) was added dropwise to a well-stirred solution of 1,4-bis[2-[2-(2-hydroxyethoxy)ethoxy]ethoxy]benzene **7** (11.6 g, 31 mmol) and freshly-distilled triethylamine (3 g, 30 mmol) in dried CH_2Cl_2 (100 mL), maintained under N_2. The mixture was stirred for 24 h at room temperature. After evaporation of the solvent under reduced pressure, the crude product was chromatographed on silica gel, eluting first with ethyl acetate/hexanes 1:1 to remove unreacted starting materials. The desired product was removed upon elution with ethyl acetate/hexanes 9:1 and was obtained as a yellow solid after removal of the solvent under reduced pressure: yield 0.8 g, 42%; mp 56−57 °C; UV−vis (CH_3CN) λ (ϵ, M^{-1} cm^{-1}) = 442 (104) nm; ^{1}H NMR (250 MHz, $CDCl_3$) δ = 3.57−3.82 (m, 18H); 4.02−4.07 (m, 4H); 4.18 (s, 5H); 4.34−4.38 (m, 4H); 4.79−4.80 (t, 2H, J = 2 Hz); 6.81 (s, 4H); ^{13}C NMR ($CDCl_3$) δ = 61.67; 63.22; 67.96; 69.42; 69.78; 69.89; 70.15; 70.30; 70.62; 70.72; 70.76; 70.86; 71.29; 72.45; 115.53; 152.95; 171.0; FAB-MS (nitrobenzyl alcohol matrix) m/z = 586 $[M]^+$; 454 $[M - C_6H_{12}O_3]^+$.

Preparation of 10. A mixture of 9-anthroyl chloride (0.6 g, 2.5 mmol) and **9** (0.5 g, 0.85 mmol) were refluxed in dried CH_3CN (50 mL) for 1 h. The solvent was removed under reduced pressure, and the residue was chromatographed on silica gel eluting with ethyl acetate/hexanes 1:1 to give a red oil: yield 0.5 g, 75%; UV−vis (CH_3CN) λ (ϵ, M^{-1} cm^{-1}) = 442 (110); ^{1}H NMR (250 MHz, $CDCl_3$) δ = 3.75−3.86 (m, 10H); 3.93−4.14 (m, 6H); 4.00−4.08 (m, 4H); 4.20 (s, 5H); 4.37−4.41 (m, 4H); 4.77−4.83 (m, 4H); 6.78 (s, 4H); 7.44−7.57 (m, 4H); 7.99−8.03 (d, 2H, J = 7.8 Hz); 8.12−8.15 (d, 2H, J = 7.8 Hz); 8.52 (s, 1H); ^{13}C NMR ($CDCl_3$) δ = 63.25; 64.53; 67.96; 68.00; 69.11; 69.46; 69.79; 69.88; 69.95; 70.18; 70.65; 70.70; 70.79; 70.80; 70.88; 71.31; 115.49; 125.16; 125.42; 126.93; 128.00; 128.57; 129.42; 130.93; 153.01; 169.42; 171.67; FAB-MS (nitrobenzyl alcohol matrix) m/z = 790 $[M]^+$; calculated for $C_{44}H_{46}O_{10}Fe$ 790.2440, found 790.2437.

Preparation of 12. A mixture of **11** (1 g, 1.6 mmol) and 9-anthroyl chloride (1.5 g, 6.2 mmol) in dried CH_3CN (50 mL) was heated to reflux for 12 h. The solvent was removed under reduced pressure, and the crude residue was chromatographed on silica gel eluting first with hexanes in order to remove unreacted starting materials. Subsequent elution with ethyl acetate removed the desired product as a yellow oil: yield 1.2 g, 75%; ^{1}H NMR (250 MHz, $CDCl_3$) δ = 3.67−3.83 (m, 26H); 3.92−4.06 (m, 10H); 4.76−4.79 (t, 4H, J = 4.6 Hz); 6.77−6.78 (m, 8H); 7.43−7.56 (m, 8H); 7.98−8.02 (d, 4H, J = 8 Hz); 8.11−8.14 (d, 4H, J = 8 Hz); 8.52 (s, 2H); FAB MS (nitrobenzyl alcohol matrix) m/z = 1051 $[M]^+$; calculated for $C_{62}H_{66}O_{15}$ 1050.4402, found 1050.4415.

Preparation of 13. A solution of ferrocenoyl chloride (2 g, 8.0 mmol) in dried CH_2Cl_2 (25 mL) was added dropwise to a stirred solution of **11** (1 g, 1.6 mmol) and triethylamine (0.8 g, 7.9 mmol) in dried CH_2Cl_2 (50 mL). The mixture was stirred for 24 h at room temperature before being washed with water (2 × 25 mL). After drying with $MgSO_4$, the solvent was removed under reduced pressure to give a red oil which was chromatographed on silica gel. Elution with CH_2Cl_2 removed several side products and unreacted starting materials, while subsequent elution with CH_2Cl_2/CH_3OH 96/4 removed the desired product as a yellow solid: yield 1.0 g, 60%; UV−vis (CH_3CN) λ (ϵ, M^{-1} cm^{-1}) = 444 (190) nm; ^{1}H NMR (250 MHz, $CDCl_3$) δ = 3.70−3.86 (m, 28H); 4.04−4.08 (t, 8H, J = 4.5 Hz); 4.20 (s, 10H); 4.37−4.41 (m, 8H); 4.81−4.83 (t, 4H, J = 2 Hz); 6.82 (s, 8H); FAB MS (nitrobenzyl alcohol matrix) m/z = 1066 $[M]^+$; calculated for $C_{54}H_{66}O_{15}Fe_2$ 1066.3100, found 1066.3102.

Preparation of 14. A solution of 4-methoxyphenol (5 g, 40 mmol) in dried *N,N*-dimethylformamide (75 mL) was added during 30 min to a stirred suspension of K_2CO_3 (44 g, 320 mmol) in dried *N,N*-dimethylformamide (75 mL) maintained under N_2. The solution was stirred for 30 min at room temperature before 2-[2-(2-chloroethoxy)-ethoxy]ethanol (13.4 g, 80 mmol) in dried *N,N*-dimethylformamide (60 mL) was added over a further 30 min. The temperature was raised to 75 °C and stirred for 7 days. After cooling to room temperature, the mixture was filtered, and the residue was washed with *N,N*-dimethylformamide (50 mL). The combined filtrates were evaporated to dryness under reduced pressure, and the residue was dissolved in CH_2Cl_2 (100 mL) before being washed with water (50 mL). After removal of the organic layer, the aqueous layer was acidified with dilute aqueous HCl and extracted with CH_2Cl_2 (2 × 100 mL). The combined organic

(16) Benniston, A. C.; Harriman, A. *Synlett* **1993**, 223.
(17) Benniston, A. C.; Harriman, A.; Lynch, V. M. *Tetrahedron Lett.* **1994**, *35*, 1473.
(18) Anelli, P. L.; Ashton, P. R.; Ballardini, R.; Balzani, V.; Delgado, M.; Gandolfi, M. T.; Goodnow, T. T.; Kaifer, A. E.; Philp, D.; Pietraszkiewicz, M.; Prodi, L.; Reddington, M. V.; Slawin, A. M. Z.; Spencer, N.; Stoddart, J. F.; Vicent, C.; Williams, D. J. *J. Am. Chem. Soc.* **1992**, *114*, 193.
(19) We are grateful for Prof. P. A. Magnus for suggesting this synthetic route and for supplying the necessary materials.
(20) Goeckner, N. A.; Synder, H. R. *J. Org. Chem.* **1973**, *38*, 481.
(21) Parrish, R. C.; Stock, M. *J. Org. Chem.* **1965**, *30*, 927.
(22) von Lorkowski, H. J.; Pannier, R.; Wendte, A. *J. Prakt. Chem.* **1967**, *35*, 149.

extracts were dried with $MgSO_4$ and evaporated to dryness on a rotary evaporator. The resultant brown oil was chromatographed on silica gel, eluting with ethyl acetate to give a yellow oil: yield 8.0 g, 78%; ^{1}H NMR (250 MHz, $CDCl_3$) δ = 3.58−3.65 (m, 4H); 3.67 (s, 3H); 3.69−3.77 (m, 4H); 3.80−3.84 (m, 2H); 4.05−4.09 (m, 2H); 6.82−6.83 (d, 4H, J = 4 Hz).

Preparation of 15. A mixture of **14** (1.0 g, 3.9 mmol) and 9-anthroyl chloride (1.4 g, 5.8 mmol) in dried CH_3CN (50 mL) was heated to reflux for 12 h. The solvent was removed under reduced pressure, and the sample was chromatographed on silica. Elution with hexanes removed various impurities before subsequent elution with hexanes/ethyl acetate 1/1 removed the desired product: yield 1.1 g, 61%; ^{1}H NMR (250 MHz, CD_3CN) δ = 3.63−3.71 (m, 9H); 3.84−3.89 (m, 4H); 4.70−4.74 (m, 2H); 6.74−6.75 (d, 4H, J = 2.3 Hz); 7.50−7.62 (m, 4H); 8.07−8.11 (d, 4H, J = 8.6 Hz); 8.64 (s, 1H); FAB MS (nitrobenzyl alcohol matrix) m/z = 461 $[M + H]^+$.

Synthesis of the [2]Rotaxanes. Preparation of 1. A mixture of **8** (1.5 g, 1.9 mmol), 1,4-bis(bromomethyl)benzene (167 mg, 0.63 mmol), **6** (450 mg, 0.63 mmol), and $AgPF_6$ (480 mg, 1.9 mmol) in dried acetonitrile (50 mL) was stirred for 7 days at room temperature. The solution was filtered before being evaporated to dryness under reduced pressure, and the residue was washed with CH_2Cl_2 (20 mL) and filtered. The residue was washed twice with CH_2Cl_2 (20 mL) before being dissolved in nitromethane (20 mL) and treated dropwise with CH_2Cl_2 until the solution became cloudy. At this point, the suspension was centrifuged, and the supernatant liquid was removed. This procedure was repeated several times on the remaining solid before the combined liquid phases were evaporated to dryness under reduced pressure at 10 °C. The crude product was purified by repeated chromatography on silica gel with CH_3OH/aqueous NH_4Cl (2M)/CH_3NO_2 7/2/1 as eluent. The product was subjected to anion exchange by stirring a solution of **1** in CH_3NO_2 with a saturated aqueous solution of NH_4PF_6. Finally, recrystallization from CH_3NO_2/diethyl ether (slow vapor diffusion) gave the required product as a red solid: yield 294 mg, 25%; UV−vis (CH_3CN) λ (ϵ, M^{-1} cm^{-1}) = 486 (560); ^{1}H NMR (500 MHz, CD_3CN) δ 2.99 (s, 4H); 3.28−3.30 (m, 4H); 3.60−3.69 (m, 4H); 3.88−3.92 (m, 8H); 4.09−4.11 (m, 4H); 4.77−4.79 (m, 4H); 5.30 (s, 8H); 6.98−7.01 (d, 8H, J = 6.9 Hz); 7.37−7.46 (m, 8H); 7.48 (s, 8H); 7.69−7.73 (d, 4H, J = 8.8 Hz); 7.75−7.78 (d, 4H, J = 8.2 Hz); 8.22 (s, 2H); 8.83−8.85 (d, 8H, J = 6.9 Hz); ^{13}C NMR (CD_3CN) δ 65.33; 67.42; 70.29; 70.59; 71.25; 71.52; 113.32; 125.29; 125.47; 127.18; 128.27; 128.70; 129.53; 130.68; 131.31; 137.11; 144.50; 145.32; 150.44; 169.07; FAB MS (nitrobenzyl alcohol matrix) m/z = 1737 $[M - PF_6]$, 1592 $[M - 2PF_6]$, 1447 $[M - 3PF_6]$; calculated for $C_{84}H_{78}N_4O_{10}F_{18}P_3$ $[M - PF_6]^+$ 1737.4643, found 1737.4682.

Preparation of 2. This material was prepared and purified as described above for **1** but using string **10** in place of **8**: yield 87.5 mg, 15%; UV−vis (CH_3CN) λ (ϵ, M^{-1} cm^{-1}) = 478 (600) nm; ^{1}H NMR (500 MHz, CD_3CN) δ = 3.19−3.20 (d, 2H, J = 9 Hz); 3.27−3.29 (d, 2H, J = 9 Hz); 3.34−3.35 (m, 2H); 3.49−3.50 (m, 2H); 3.72−3.74 (m, 2H); 3.83−3.85 (m, 2H); 3.91−3.96 (m, 10H); 4.13−4.17 (m, 2H); 4.18 (s, 5H); 4.29−4.31 (m, 2H); 4.36−4.38 (m, 2H); 4.58−4.59 (m, 2H); 4.80−4.82 (m, 2H); 5.42−5.45 (d, 4H, J = 13.4 Hz); 5.52−5.55 (d, 4H, J = 13.4 Hz); 7.36−7.37 (d, 8H, J = 7 Hz); 7.39−7.43 (d,t, 2H, J = 5.6 Hz, J' = 1 Hz); 7.47−7.50 (d,t, 2H, J = 6.5 Hz, J' = 1.2 Hz); 7.63 (s, 8H); 7.74−7.76 (d,d, 2H, J = 8.7 Hz, J' = 1 Hz); 7.79−7.82 (d, 2H, J = 8.7 Hz); 8.26 (s, 1H); 8.58−8.59 (d, 8H); FAB MS (nitrobenzyl alcohol matrix) m/z = 1746 $[M - PF_6]^+$; calculated for $C_{80}H_{78}N_4O_{10}F_{18}P_3Fe$ $[M - PF_6]^+$ 1745.3993, found 1745.4008.

Preparation of 4. A mixture of **13** (1.0 g, 0.94 mmol), 1,4-bis-(bromomethyl)benzene (83 mg, 0.31 mmol), **6** (220 mg, 0.31 mmol), and $AgPF_6$ (240 mg, 0.94 mmol) in dried acetonitrile (50 mL) was stirred for 7 days at room temperature. The solution was filtered before being evaporated to dryness under reduced pressure, and the residue was washed with CH_2Cl_2 (20 mL) and filtered. The residue was washed twice with CH_2Cl_2 (20 mL) before being dissolved in nitromethane (20 mL) and treated dropwise with CH_2Cl_2 until the solution became cloudy. At this point, the suspension was centrifuged, and the supernatant liquid was removed. This procedure was repeated several times on the remaining solid before the combined liquid phases were evaporated to dryness under reduced pressure at 10 °C. The crude product was purified by repeated chromatography on silica gel with CH_3OH/aqueous NH_4Cl (2M)/CH_3NO_2 7/2/1 as eluent. The product was subjected to anion exchange by stirring a solution of **4** in CH_3NO_2 with a saturated aqueous solution of NH_4PF_6. Finally, recrystallization from CH_3NO_2/diethyl ether (slow vapor diffusion) gave the required product as a red solid: yield 67 mg, 10%; UV−vis (CH_3CN) λ (ϵ, M^{-1} cm^{-1}) = 467 (1000) nm; ^{1}H NMR (500 MHz, acetone-d_6 298 K) δ = 3.61−4.04 (m, 44H); 4.18 (s, 10H); 4.31−4.40 (m, 8H); 4.66 (br, 4H); 6.03 (s, 8H); 8.03 (s, 8H); 8.19−8.20 (d, 8H, J = 6.6 Hz); 9.30−9.32 (d, 8H, J = 6.5 Hz); ^{1}H NMR (500 MHz, acetone-d_6, 213 K): 3.32−3.38 (m, 2H); 3.47−3.50 (m, 4H); 3.58−3.76 (m, 20H); 3.89−4.08 (m, 14H); 4.09 (s, 5H); 4.18−4.19 (m, 2H); 4.20 (s, 5H); 4.26−4.27 (m, 2H); 4.12−4.19 (t, 2H, J = 1.7 Hz); 4.43−4.44 (t, 2H, J = 1.6 Hz); 4.45−4.60 (m, 2H); 4.71−4.72 (t, 2H, J = 1.7 Hz); 5.97 (s, 8H); 6.29−6.39 (d,d, 4H, J = 4.4 Hz, J' = 9 Hz); 7.98 (s, 4H); 8.03 (s, 4H); 8.16−8.19 (m, 8H); 9.31−9.33 (m, 8H); FAB MS (nitrobenzyl alcohol matrix) m/z = 2023 $[M - PF_6]^+$; 1877 $[M - 2PF_6]^+$; 1732 $[M - 3PF_6]^+$; calculated for $C_{90}H_{98}N_4O_{15}F_{18}P_3Fe_2$ $[M - PF_6]^+$ 2021.4653, found 2021.4603.

Preparation of 5. Prepared and purified as described above for **4** but using string **12** in place of **13**: yield 290 mg, 36%; UV−vis (CH_3CN) λ (ϵ, M^{-1} cm^{-1}) = 485 (990) nm; ^{1}H NMR (500 MHz, acetone-d_6, 243 K) δ = 3.35−3.49 (m, 10H); 3.50 (m, 2H); 3.58−3.59 (m, 2H); 3.68−3.77 (m, 14H); 3.81−3.82 (m, 2H); 3.88−3.91 (m, 8H); 4.27 (m, 2H); 4.78 (m, 2H); 4.91 (m, 2H); 5.69−5.77 (d,d, 8H, J = 22 Hz, J' = 13 Hz); 6.29−6.37 (d,d, 4H, J = 28 Hz, J' = 9 Hz); 7.32−7.34 (t, 2H, J = 7.5 Hz); 7.44−7.48 (m, 2H); 7.51−7.55 (m, 2H); 7.57−7.59 (t, 2H, J = 7.7 Hz); 7.63−7.65 (d, 4H, J = 6.3 Hz); 7.69−7.71 (d, 2H, J = 7.5 Hz); 7.73 (s, 4H); 7.75−7.76 (d, 4H, J = 6.4 Hz); 7.79 (s, 4H); 7.79−7.81 (d, 2H, J = 8.8 Hz); 8.07−8.08 (d, 2H, J = 8.8 Hz); 8.09−8.11 (d, 2H, J = 8.5 Hz); 8.13 (s, 1H); 8.67 (s, 1H); 8.86−8.87 (d, 4H, J = 6.0 Hz); 9.03−9.04 (d, 4H, J = 6.4 Hz); FAB MS (nitrobenzyl alcohol matrix) m/z = 2007 $[M - PF_6]^+$; 1862 $[M - 2PF_6]^+$; 1716 $[M - 3PF_6]^+$; calculated for $C_{98}H_{98}N_4O_{15}P_3F_{18}$ $[M - PF_6]^+$ 2005.5942, found 2005.5942.

X-ray Crystallography. X-ray experimental for $C_{78}H_{86}N_4O_{15}P_4F_{24}Fe_2$ **3**: Large red, block-like crystals were obtained by vapor diffusion of diethyl ether into a nitromethane solution of **3** maintained at 273 K.

X-ray experimental for $C_{90}H_{84.5}N_{5.5}O_{13.5}P_{3.5}F_{21.5}$ **1**: Red, block-like crystals were obtained by cooling a hot saturated solution of **1** in $CH_3OH/NH_4Cl(aq)/CH_3NO_2$.

The crystals were very sensitive to decomposition due to loss of solvent of crystallization when removed from the mother liquor. The data were collected at 173 K on a Nicolet P3 diffractometer, equipped with a Nicolet LT-2 low temperature device and using a graphite monochromater with Mo Kα radiation (λ = 0.71073 Å). Details of crystal data, data collection, and structure refinement are listed in Table 1. Four check reflections were remeasured every 96 reflections to monitor instrument and crystal stability. A smoothed curve of the intensities of these check reflections was used to scale the data. The scaling factor ranged from 0.99 to 1.01 for **1** and from 0.994 to 1.02 for **3**. The data were corrected for Lp effects but not for absorption. Data reduction and decay correction were performed using the SHELXTL-*Plus* software package.[23] The structures were solved by direct methods and refined by full-matrix, least-squares iteration.[23] Because of the large number of atoms in the structure and the low data-to-parameter ratio, only selected non-hydrogen atoms were refined anisotropically. For **1**, the atoms of the full occupancy PF_6^- groups were refined anisotropically and all other non-hydrogen atoms were refined isotropically. For **3**, most non-hydrogen atoms were refined anisotropically. The hydrogen atoms were calculated in idealized positions with isotropic temperature factors fixed at 0.08.

Two independent structures were resolved for [2]rotaxane **1**; both lie around crystallographic inversion centers and are well behaved. One of the four PF_6^- groups (P4, F19−24) is poorly resolved and is found in a region of the cell containing poorly resolved solvent. After many unsuccessful attempts to work out the solvent disorder, it was decided to try to account for the electron density in this region by assigning atoms to the largest peaks without recourse to geometric constraints. In **3**, the [2]rotaxane lies around an inversion center at 1/2, 0, 1. One PF_6^- group is partially disordered by rotation about a linear F−P−F vector so that two fluorine atoms (F1 and F2) were of full occupancy and the remaining four (F3−F6 and F3a−F6a) had partial occupancy.

(23) Sheldrick, G. M. *SHELXTL-Plus (Version 4.11)*; Siemens X-ray Analytical Instruments Inc.: Madison, WI, 1991.

Table 1. Crystallographic Data[a] Collected for Compounds $[(C_{48}H_{46}O_{10})(C_{36}H_{32}N_4)]^{4+}(PF_6^-)_{3.5}\ (F^-)_{0.5}(CH_3NO_2)_{1.5}\cdot{}^1/_2H_2O\cdot 4C^d$ (**1**) and $[(C_{40}H_{46}O_{10}Fe_2)(C_{36}H_{32}N_4)]^{4+}(PF_6^-)_4(CH_3NO_2)_2\cdot H_2O$ (**3**)

	1	**3**
formula	$C_{90}H_{84.5}N_{5.5}O_{13.5}P_{3.5}F_{21.5}$	$C_{78}H_{86}N_6O_{15}P_4F_{24}Fe_2$
fw	1976	2039.12
a, Å	14.112(2)	15.746(4)
b, Å	16.229(2)	12.521(3)
c, Å	20.759(3)	22.778(6)
α, deg	95.537(13)	90.0
β, deg	92.726(13)	107.98(2)
γ, deg	94.420(13)	90.0
V, Å^3	4709	4272(2)
Z	2	2
F(000)	2034	2088
space group	$P\bar{1}$	$P2_1/n$
ϱ_{calc}, g/cc	1.39	1.58
radiation	graphite monochromatized, Mo Kα (λ = 0.71073 Å)	
μ, cm^{-1}	1.7	5.277
transmission factor[b] range	not applied	0.8280−0.9029
$R(F)$[c]	0.116	0.104
$R_w(F)$	0.145	0.0857
S, goodness of fit	3.486	1.913

[a] Data for both samples were collected on a Nicolet P3 diffractometer. Data for **1** and **3** were collected at −100 °C, while using a Nicolet LT-2 low-temperature delivery system. Lattice parameters were obtained from the least-squares refinement of 38 reflections with $12.5 < 2\theta < 17.8°$ for **1** and 50 reflections with $12.3 < 2\theta < 24.0°$ for **3**. [b] Absorption correction was based on measured crystal faces. [c] The function, $\sum w(|F_o| - |F_c|)^2$, was minimized and where $w = 1/(\sigma(F_o)^2 + (0.02F)^2)$. $R(F) = \sum(|F_o| - |F_c|)/\sum|F_o|$. $R_w(F) = [\sum w(|F_o| - |F_c|)^2/\sum w(|F_o|)^2]^{1/2}$. $S = [\sum w(|F_o| - |F_c|)^2/(m - n)]^{1/2}$, where *m* is the number of reflections used during refinement and *n* is the number of parameters refined. [d] The structural formula could not be determined exactly because of regions of highly disordered solvent and one partial occupancy PF_6^- group.

The site occupancy factor refined to 51(1)% and was fixed at 50% for the remainder of the refinement.

The function, $\sum_w(|F_o|) - (|F_c|)^2$ was minimized, where $w = 1/(\sigma F_o)^2$ and $\sigma F_o = [0.5\{(kI) - \{(\sigma I)^2 + (0.02I)^2\}^{1/2}\}]$. The intensity *I* is given by $I = [(I_{peak} - I_{background}) \times (\text{scan rate})]$. The factor 0.02 is to downweight intense reflections and to account for instrument instability and *k* is the correction due to Lp effects and decay. $\sigma(I)$ was estimated from counting statistics: $\sigma(I) = [(I_{peak} - I_{background})^{1/2} \times (\text{scan rate})]$. Neutral atom scattering factors for the non-hydrogen atoms were taken from Cromer and Mann,[24] with the anomolous-dispersion corrections taken from the work of Cromer and Liberman.[25] The scattering factors for the hydrogen atoms were obtained from Stewart *et al.*;[26] and values used to calculate the linear absorption coefficient were taken from the International Tables for X-ray Crystallography (1974).[27] Other computer programs used in this work are listed elsewhere.[28] All figures were generated using SHELXTL-*Plus*.[23] Tables of positional and thermal parameters, bond lengths, angles and torsional angles, figures, and lists of observed and calculated structure factors are located in the supplementary material.

Instrumentation. FAB-MS were obtained on a Finnigan MAT TSQ0-70 instrument as *m*-nitrobenzyl alcohol matrices. ^{1}H NMR spectra were recorded with Bruker AC250 or General Electric GN-500 FT-NMR instruments with TMS as internal standard. All solvents used for NMR studies were dried over activated molecular sieves prior to use in the variable temperature experiments. Temperatures were measured using a calibrated probe and were accurate to ±1 °C of the quoted value. Thermodynamic and kinetic data corresponding to the shuttling processes evident in [2]rotaxanes **4** and **5** were calculated using standard methodology. Peak locations and half-widths were obtained from appropriate spectra by computer curve fitting routines.

Absorption spectra were recorded with Hewlett Packard 8450A or Hitachi U-3210 spectrophotometers, while fluorescence spectra were recorded on a fully-corrected Perkin Elmer LS-5 spectrofluorimeter. Solutions for fluorescence studies were adjusted to possess an absorbance of <0.10 at the excitation wavelength. Electrochemical measurements were made on a Pine Instruments model AFRDE 4 potentiostat coupled to a standard X-Y recorder. Solutions of the compound (1 mM) in dried acetonitrile containing tetra-*N*-butylammonium perchlorate (0.2 M) were purged thoroughly with N_2 before electrolysis. A glassy carbon microdisc was used as working electrode, in conjunction with a Pt wire counter electrode and an SCE reference electrode. All reported redox potentials were reproducible to ±10 mV.

Fluorescence lifetimes were measured by time-correlated, single-photon counting techniques using a mode-locked, synchronously pumped, cavity-dumped Rhodamine 6G dye laser as excitation source. The excitation wavelength was 305 nm and fluorescence was isolated from scattered laser light with a high radiance monochromator, used in conjunction with glass cut-off filters. The instrument response function (FWHM ≈ 60 ps) was deconvoluted from the experimental decay profile prior to data analysis. The ultimate time resolution of this setup, applying global analysis methodology, was *ca.* 20 ps. Flash photolysis studies were made with a frequency-doubled, mode-locked Antares 76S Nd:YAG laser as excitation source for a synchronously pumped Styryl-9 dual-jet dye laser. Output from the dye laser, which was tuned to 880 nm (FWHM = 350 fs, pulse energy 600 μJ) was amplified, autocorrelated, and used to generate a white light continuum by focussing into CS_2. Part of the laser output was frequency-doubled and used as excitation pulse. The monitoring pulse was optically delayed and transient differential absorption spectra were recorded with an intensified Princeton dual-diode array fitted to a Spex spectrograph. Approximately 500 individual shots were averaged for each time delay and analyzed by computer nonlinear least-squares iteration. Kinetic studies were made by overlaying spectra collected at about 30 different delay times. For long-lived transient species, the excitation pulse was provided from a frequency-doubled, mode-locked Quantel YG402 Nd:YAG laser (pulse duration 30 ps) after Raman shifting to 440 nm. A pulsed Xe arc lamp was used as monitoring pulse, and kinetic studies were made at fixed wavelength with 50 individual laser shots being averaged. After correction for changes in the baseline, the signal was analyzed by computer nonlinear least-squares iteration.

Results and Discussion

Synthesis of [2]Rotaxanes. The various [2]rotaxanes studied here may be conveniently categorized as containing one or two dialkoxybenzene subunits per string and are termed, respectively, one-station or two-station [2]rotaxanes; structures are shown in Figure 1. Each of the [2]rotaxanes was prepared by the template method developed earlier by Stoddart and co-workers[29] and used previously for preparation of **3**.[15] Preparation of the two-station [2]rotaxanes **4** and **5** was accomplished using an excess of the appropriate string in order to prevent attaching two molecules of cyclophane to the string. The stoppered strings **8** and **10**, shown in Figure 2, were prepared from the diol **7** using standard organic reactions. Reaction of excess 9-anthroyl chloride with **7** in acetonitrile gave, after work up and purification by chromatography on silica gel, the string having an anthracene moiety at each end (**8**). In order to obtain only the monofunctionalized string **9**, excess **7** was stirred for 24 h in dichloromethane with ferrocenoyl chloride and triethylamine. The desired product was easily separated from unreacted **7** by silica gel column chromatography. Refluxing **9** in acetonitrile containing a slight excess of 9-anthroyl chloride for 1 h gave the corresponding asymmetric string **10** in 75% yield. Compound **11** was synthesized using 20% $Pd(OH)_2$ on activated carbon in cyclohexene to remove the protective group,[19] rather than H_2 over palladium since, although both methods gave almost quantitative yields, the former was easier to execute. For complete understanding of the fluorescence quenching data, it was necessary to synthesize **14** as a reference compound. Synthesis was carried out using two straightforward organic reactions starting from the readily available 4-methoxyphenol.

(24) Cromer, D. T.; Mann, J. B. *Acta Crystallogr.* **1968**, *A24*, 321.
(25) Cromer, D. T.; Liberman, D. *J. Chem. Phys.* **1970**, *53*, 1891.
(26) Stewart, R. F.; Davidson, E. R.; Simpson, W. T. *J. Phys. Chem.* **1965**, *42*, 3175.
(27) *International Tables for X-ray Crystallography*; Kynoch Press, Birmingham, 1974; Vol. IV, p 55.
(28) Gadol, S. M.; Davis, R. E. *Organometallics* **1982**, *1*, 1607.

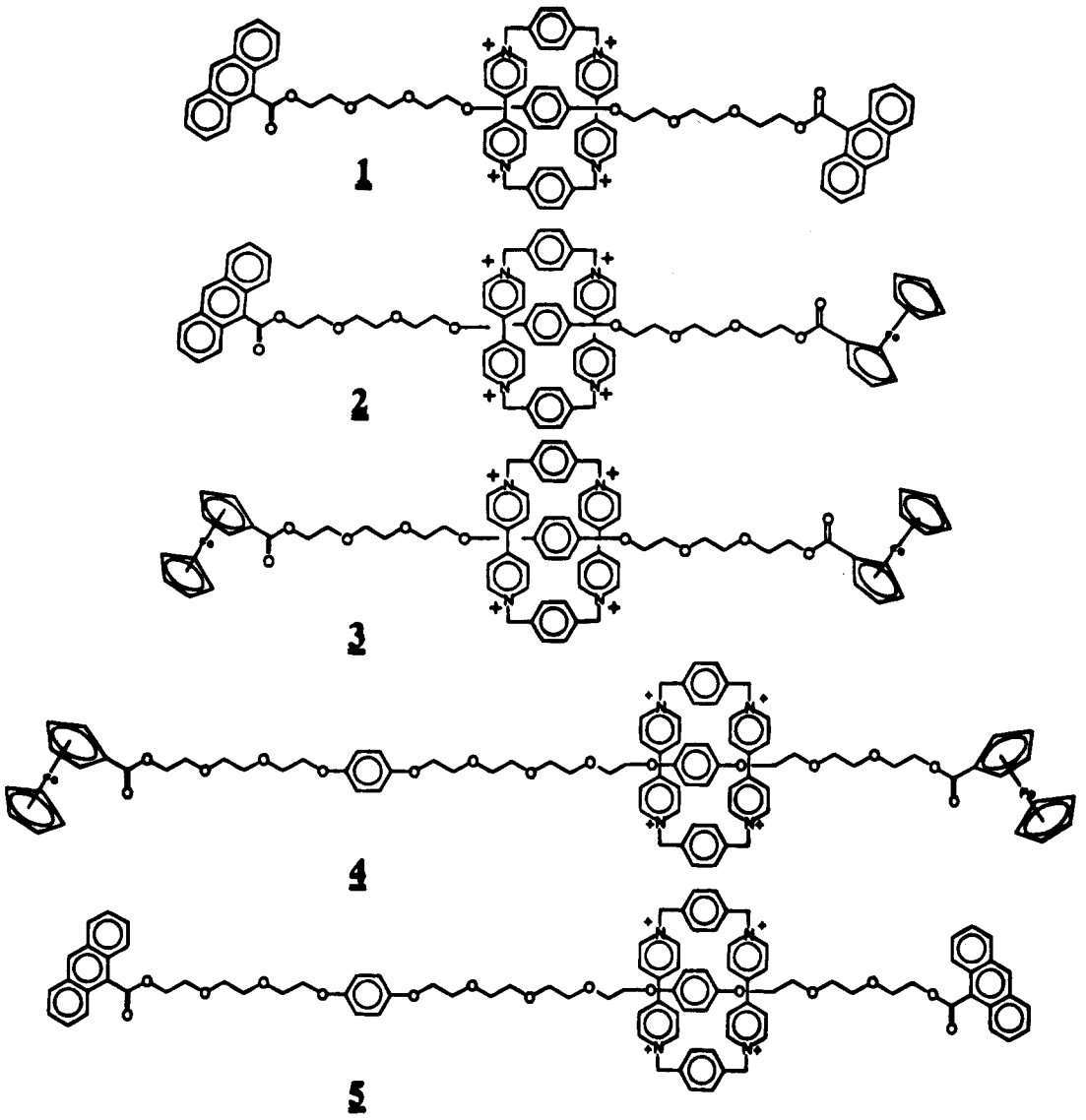

Figure 1. Structures of the various [2]rotaxanes studied in this work.

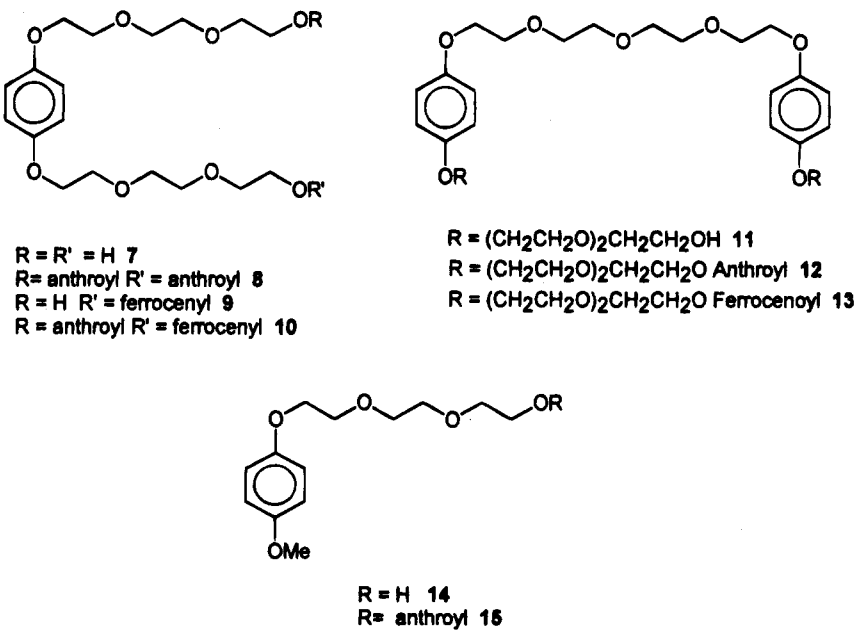

Figure 2. Structures of the strings and reference compounds used in this work.

X-ray Crystallographic Structures of [2]Rotaxanes 1 and 3. The crystal structures of numerous closely-related cyclophanes, [2]rotaxanes, and catananes have been described in recent years,[18,29-31] and, as a consequence, much is now known about the mutual interaction between donor and acceptor subunits. During the course of this investigation, we were able

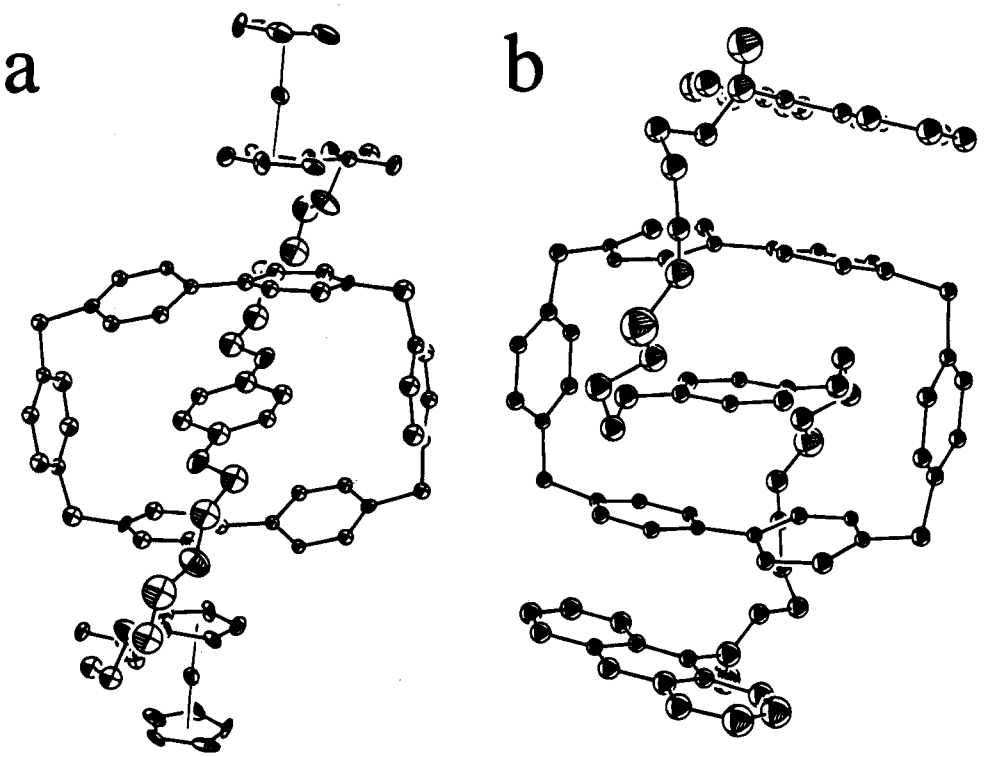

Figure 3. X-ray crystal structure obtained for (a) **3** and (b) **1**. Hexafluorophosphate groups have been omitted for clarity of presentation.

to crystallize the symmetrical [2]rotaxanes **1** and **3** and to study their structures by X-ray crystallography. The most significant finding is that, in both cases, the terminal stoppers are closely-associated with the central cyclophane in the solid state. A similar conclusion was raised for pseudorotaxanes where dialkoxybenzene or dialkoxynaphthalene groups incorporated into the string were found to align with the cyclophane.[32] Both anthracene and ferrocene moieties are held in van der Waals contact with one of the pyridinium rings comprising the cyclophane, which itself is centralized over the dialkoxybenzene group. This preorganization, which according to NMR and time-resolved fluorescence spectroscopy persists in acetonitrile and acetone solutions, is of major importance in facilitating the electron-transfer pathway that leads to formation of spatially-remote redox equivalents. Indeed, without the π-stacking between stopper and cyclophane it is unlikely that sequential electron transfer could occur.[17]

In agreement with earlier investigations on related structures,[18,29-32] it was observed that the central dialkoxybenzene subunit in the [2]rotaxanes **1** and **3** is positioned at the center of the cyclophane. In [2]rotaxane **3** the phenyl ring lies on a center of symmetry, with the center of the phenyl ring being held 3.51 Å from the center of the adjacent 4,4′-bipyridinium subunit (Figure 3a). The angle of tilt of the phenyl ring with respect to the center of the cyclophane is 79.1°. The dimensions of the cyclophane are 10.17 Å × 7.01 Å, while the dihedral angle between the pyridinium rings of the 4,4′-bipyridinium dication is 23.1°. Thus, the two pyridinium rings are nonplanar. For the corresponding anthracene-stoppered [2]rotaxane **1** two different orientations are present in the unit cell (Figure 4). One of these structures (designated **1a**) appears very similar to that found for **3**, except that the dihedral angle of the pyridinium rings in the cyclophane is only 17.4°, and the tilt angle is reduced to 51.7° (Figure 3b). The second of these structures (i.e., **1b**) shows an elongated cyclophane having dimensions of 10.30 Å × 6.97 Å. The central phenyl ring lies closer to the center of the 4,4′-bipyridinium dications, the separation being 3.48 Å, while the tilt angle of 46.5° is substantially less than those found for the other structures. The dihedral angle between the pyridinium rings in the cyclophane is 20.9° and is slightly larger than found for **1a**.

The proximal cyclopentadienyl ring on each of the terminal ferrocene subunits in [2]rotaxane **3** is positioned within van der Waals contact of a pyridinium ring on the central cyclophane (Figure 3a). The closest approach between these subunits is 3.32 Å, the corresponding distance between the center of the cyclopentadienyl ring and the center of the 4,4′-bipyridinium dication being 3.50 Å, while the dihedral angle between the π-stacking subunits is only 5.6°. This represents a displacement of 1.10 Å from the idealized position. Similarly, in **1a** the anthracene moieties are closely associated (i.e., 3.45 Å) with one of the pyridinium rings comprising the cyclophane. The distance between the center of the anthracene ring and the center of the 4,4′-bipyridinium dication is 3.64 Å, while the dihedral angle between the π-stacking groups is 11.6° (Figure 3b). Although this angle is significantly larger than that found for **3** the positioning of the subunits is only 1.16 Å away from ideality. For **1b**, there is more pronounced orbital overlap between each terminal anthracene and its complementary pyridinium subunit, since the separation distance is only 3.33 Å. In this structure, the interplanar dihedral angle is only 2.5°, and, consequently, the rings are almost coplanar.

The ferrocene-stoppered [2]rotaxane **3** does not exhibit multiple π-stacking throughout the crystal lattice. However, [2]rotaxane **1** shows extended π-stacking along a single axis (Figure 4). Thus, the terminal anthracene groups in **1b**, which are aligned with the *N,N′*-bipyridinium subunits of the central

(29) Philp, D.; Stoddart, J. F. *Synlett* **1991**, 445 and references therein.
(30) (a) Ashton, P. R.; Grognuz, M.; Slawin, A. M. Z.; Stoddart, J. F.; Williams, D. J. *Tetrahedron Lett.* **1991**, *32*, 6235. (b) Ashton, P. R.; Brown, C. L.; Chrystal, E. J. T.; Goodnow, T. T.; Kaifer, A. E.; Parry, K. P.; Slawin, A. M. Z.; Spencer, N.; Stoddart, J. F.; Williams, D. J. *Angew. Chem., Int. Ed. Engl.* **1991**, *30*, 1039.
(31) Ashton, P. R.; Odell, B.; Reddington, M. V.; Slawin, A. M. Z.; Stoddart, J. F.; Williams, D. J. *Angew. Chem., Int. Ed. Engl.* **1988**, *27*, 1550.
(32) (a) Anelli, P. L.; Ashton, P. R.; Spencer, N.; Slawin, A. M. Z.; Stoddart, J. F.; Williams, D. J. *Angew. Chem., Int. Ed. Engl.* **1991**, *30*, 1036. (b) Ashton, P. R.; Philp, D.; Spencer, N.; Stoddart, J. F.; Williams, D. J. *J. Chem. Soc., Chem. Commun.* **1994**, 181.

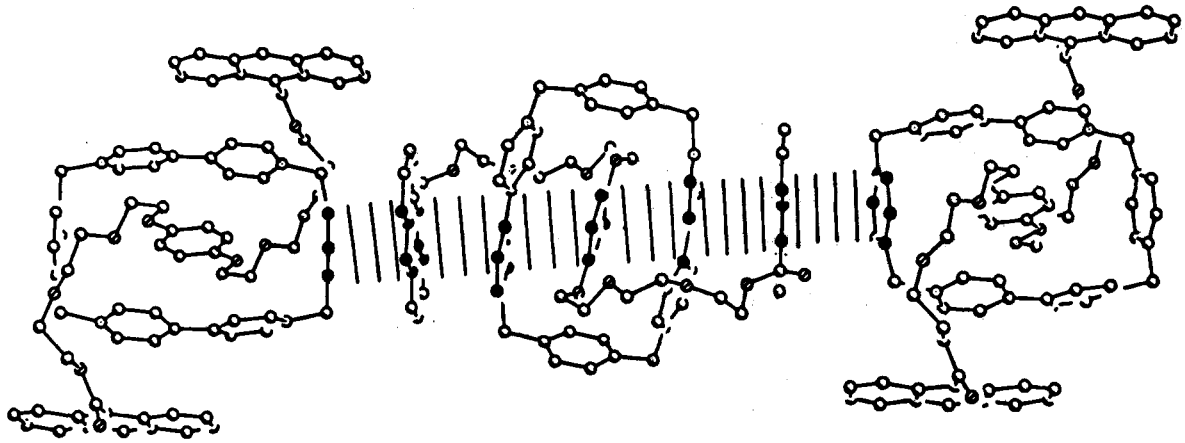

Figure 4. Crystal packing diagram obtained for **1** showing extended π-stacking along a single axis. As described in the text, structure **1a** refers to the exterior molecules while **1b** refers to the central molecule.

cyclophane, are seen to closely-associate with the xylyl groups of neighboring [2]rotaxane molecules. The intermolecular distance between these rings is 3.65 Å, indicating that they lie within van der Waals contact. Intermolecular association of this type explains why the cyclophane in **1b** appears to be elongated since the molecule is effectively squashed by its neighbors. This limited π-stacking appears to align seven aromatic rings, localized on three different molecules and involving six separate subunits, into a stack. It is interesting to note that a closely-related pseudorotaxane having dialkoxynaphthalene groups built into the string forms an intermolecular stack in the crystal lattice that aligns six aromatic rings.[32]

^{1}H NMR Spectral Studies with the One-Station [2]-Rotaxanes 1−3. Previous work[18,29-32] has established criteria allowing for full interpretation of the ^{1}H NMR spectra of the one-station [2]rotaxanes, and, therefore, assignment of the spectral parameters for **1−3** was relatively straightforward. Selected chemical shifts for the aromatic residues in [2]rotaxanes **1−3** are given in Table 2. Previously, it was demonstrated that the CH(α) and CH(β) protons on the 4,4′-bipyridinium dication subunits comprising the cyclophane undergo slight downfield and significant upfield shifts, respectively, upon incorporation of a dialkoxybenzene donor into the cavity of the cyclophane[18,29,33] Similar behavior is observed when a 4,4′-bipyridinium dication and a dialkoxybenzene group are incorporated into the same macrocyclic ring.[34] However, for each of the [2]rotaxanes **1−3** it was observed that both the CH(α) and CH(β) protons were located well upfield of the corresponding signals found for the charge-transfer complex formed between the cyclophane and 1,4-dimethoxybenzene in the same solvent (Table 2). Clearly, some additional interaction must persist in the [2]rotaxanes that is not apparent in the unstoppered cyclophane-derived system.

The most likely explanation for these upfield shifts is that the cyclophane falls within a shielding zone exerted by the terminal aromatic stoppers. Indeed, unequivocal evidence for intramolecular π-stacking between these subunits in the solid state is indicated by X-ray crystallography. Significant upfield shifts are also observed for protons located on the ferrocene and anthracene subunits that form the terminal stoppers for [2]-rotaxanes **1−3** (Table 2). From the magnitude of the shifts observed for the CH(β) protons of the 4,4′-bipyridinium dication subunits (e.g., **1** $\Delta\delta = -0.90$; **2** $\Delta\delta = -0.53$; and **3** $\Delta\delta = -0.17$), it can be surmised that anthracene exerts a more powerful shielding effect than does ferrocene. This may be due to the increased surface area of anthracene, to stereochemical factors associated with attaining a planar arrangement of the aromatic rings, or to anthracene showing more affinity to associate with the cyclophane.

Table 2. Selected ^{1}H NMR Chemical Shifts for the Various [2]Rotaxanes and Their Precursors as Observed in CD_3CN at 25 °C[e]

compd	4,4′-bipyridinium α[c]	4,4′-bipyridinium β[d]	ferrocene			anthracene H(10)
9			4.74	4.41	4.19	
ethyl anth[a]						8.61
pseudorot[b]	8.92	7.89				
1	8.33	6.99				8.22
	(−0.59)	(−0.90)				(−0.39)
2	8.59	7.36	4.58	4.37	4.18	8.26
	(−0.33)	(−0.53)	(−0.16)	(−0.04)	(−0.01)	(−0.35)
3	8.85	7.72	4.52	4.27	4.16	
	(−0.07)	(−0.17)	(−0.22)	(−0.14)	(−0.03)	

[a] Ethyl-9-anthroate. [b] Pseudorotaxane formed between the cyclophane and string **7**. [c] Refers to H(2,6,2′,6′). [d] Refers to H(3,5,3′,5′). [e] The difference in chemical shift between the compound and its respective control is given in parentheses. All chemical shifts are in ppm with TMS as reference.

Even on the NMR time scale, the conformation of these [2]-rotaxanes should be considered as existing in a state of flux,[29] not only can the terminal groups associate with the cyclophane or remain free in solution but also the cyclophane itself can migrate incoherently along the extended string[33b] (Figure 5). Indeed, close inspection of the aromatic proton spectral region for [2]rotaxane **3** in CD_3CN solution showed the existence of two matching sets of signals associated with the 4,4′-bipyridinium dication and xylyl subunits of the cyclophane (Figure 6). Integration of these two sets of signals, as observed at −35 °C where the signals are well resolved, gave an approximate ratio of 2.5 in favor of the upfield protons. The absence of a signal with $\delta \approx 6.80$, which is characteristic of the unbound dialkoxybenzene subunit, is inconsistent with one set of signals being due to free cyclophane, as might arise from dissociation of the [2]rotaxane. Signals attributable to the ferrocene subunit also appeared as two matching sets, with those of the minor component having the appearance of the isolated string **9**. Since neither repeated recrystallization of the sample nor taking crystals used for X-ray crystallography altered the spectrum, it is unlikely that the additional peaks are due to the presence of impurities. With increasing temperature, the two sets of matching signals approached coalescence (Figure 6), although the peaks were still partially resolved at 50 °C, and the relative integral increased in favor of the set of peaks located more upfield.

(33) (a) Goodnow, T. T.; Reddington, M. V.; Stoddart, J. F.; Kaifer, A. E. *J. Am. Chem. Soc.* **1991**, *113*, 4335. (b) Anelli, P. L.; Spencer, N.; Stoddart, J. F. *J. Am. Chem. Soc.* **1991**, *113*, 5131. (c) Cordova, E.; Bissell, R. A.; Spencer, N.; Ashton, P. R.; Stoddart, J. F.; Kaifer, A. E. *J. Org. Chem.* **1993**, *58*, 6550. (d) Gunter, M. J.; Johnson, M. R. *J. Chem. Soc., Chem. Commun.* **1994**, 829.

(34) Benniston, A. C.; Harriman, A. *J. Am. Chem. Soc.* **1994**, *116*, 11531.

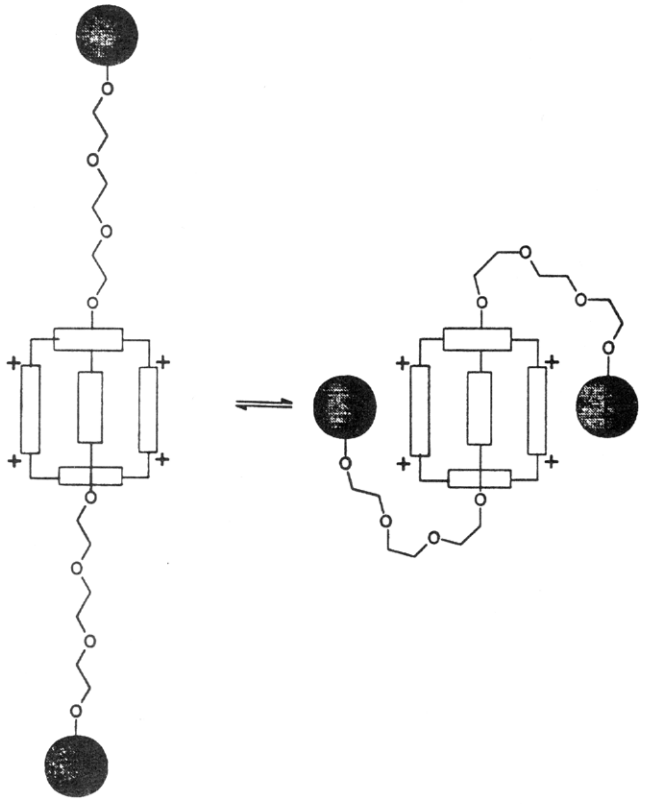

Figure 5. Major conformational exchange process for the one-station [2]rotaxanes. The cyclophane can oscillate along the extended string in the "open" conformer while the terminal stoppers associate with the exterior of the cyclophane in the "closed" conformer.

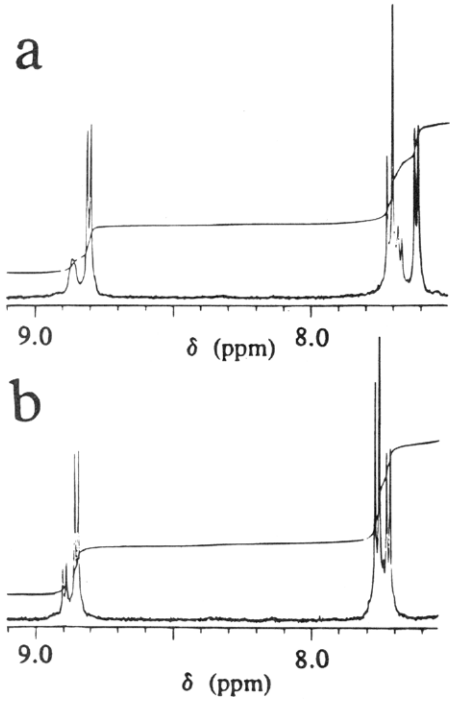

Figure 6. Partial ^{1}H NMR (500 MHz) spectra recorded for **3** in CD_3CN at (a) −35 °C and (b) +25 °C showing the aromatic region.

On this basis, we interpret these two sets of signals observed for **3** as being indicative of the existence of two families of conformations; one fmaily having the terminal ferrocene π-stacked to the cyclophane (i.e., the more downfield shifted peaks) and the second family having the subunits kept remote (i.e., the more upfield shifted peaks). Over the temperature range studied (i.e., −35 to +50 °C) the limiting values of the chemical shifts for these two conformers could not be identified. However, assuming the association constant is equal to the ratio of the integrals for "closed" and "open" conformers, the association constant at 25 °C was estimated as 0.36 (i.e., $\Delta G^\circ \approx 2.5$ kJ mol^{-1}). From the Gibbs−Helmholtz expression, the changes in enthalpy and entropy associated with formation of the "closed" conformer were estimated as 1.5 kJ mol^{-1} and −14 J mol^{-1} K^{-1}, respectively. The modest enthalpy change seems appropriate for weak π-stacking,[35] while the large entropy change corresponds to inhibition of rotational degrees of freedom associated with the string.

Interestingly, [2]rotaxane **1**, which has two terminal anthracene stoppers, does not show a second set of resonances in the aromatic region. This may indicate that the anthracene stoppers favor a closed conformation. For **1** in CD_3CN at 25 °C, rotating frame nuclear Overhauser effect spectroscopy (ROESY) measurements showed clear nuclear Overhauser effects (NOE) between the CH(β) protons on the cyclophane and the H(1,8), H(4,5), and H(10) protons on the terminal anthracene stoppers (Figure 7). This finding, taken together with time-resolved fluorescence spectroscopy (see later), appears consistent with effective π-stacking between cyclophane and stopper. We consider, therefore, that these anthracene-stoppered [2]rotaxanes exist primarily in the form of closed conformations in both solution and solid phases.

The string in [2]rotaxane **2** is asymmetric, and, as a consequence, there are some interesting NMR splitting patterns. In particular, a prochiral center is generated at the methylene bridge of the cycloplane. These methylene protons appear as a singlet with $\delta \approx 5.70$ in [2]rotaxanes **1** and **3** but for **2** they take the form of an AA′BB′ pattern with $\delta = 5.43$ ($J = 13.4$ Hz) and 5.54 ($J = 13.4$ Hz), as shown in Figure 8. The asymmetry of the string also causes protons resident on the bound dialkoxybenzene group to display an AA′BB′ pattern with $\delta = 3.20$ ($J = 9$ Hz) and 3.28 ($J = 9$ Hz). It should be noted that the asymmetry of string does not in itself affect the ^{1}H NMR pattern of the dialkoxybenzene group since this appears as a singlet ($\delta \approx 6.8$) in the uncomplexed string **10**. Therefore, the asymmetry observed for **2** is induced by close association of the two dissimilar terminal stoppers with the central cyclophane.

^{1}H NMR Spectral Studies with the Two-Station [2]-rotaxanes 4 and 5. Incorporation of a second degenerate state into the string of the above [2]rotaxanes provides for increased migration of the cyclophane along the string and for adoption of more complex conformations in solution. Indeed, prior work[29,33b] has established that the cyclophane can oscillate between the two stations on the NMR time scale, and both kinetic and thermodynamic studies have been completed for several such systems. The presence of a second (identical) donor in the string for [2]rotaxanes **4** and **5** makes for a particularly complicated structure since intramolecular π-stacking might interfere with oscillation of the cyclophane along the string. Indeed, a crude working model for the primary dynamical processes expected for such systems on the NMR time scale is presented as Figure 9.

At 25 °C in acetone-d_6, [2]rotaxane **4** exhibits a relatively simple NMR spectrum. In particular, the resonances for protons on the distal cyclopentadienyl ring of the ferrocene subunits appear as a singlet at $\delta = 4.18$; a value similar to that found for **3**. The broad resonance observed at $\delta \approx 4.6$ arises from overlap of signals due to the two equivalent H(2,5) protons on the proximal cyclopentadienyl ring of each ferrocene subunit, indicating near equivalence of the two ferrocenes. Signals for the CH(α) and CH(β) protons on the 4,4′-bipyridinium dications of the cyclophane are situated very close ($\Delta\delta \approx 0.05$) to the corresponding signals observed for the one-station analogue **3**.

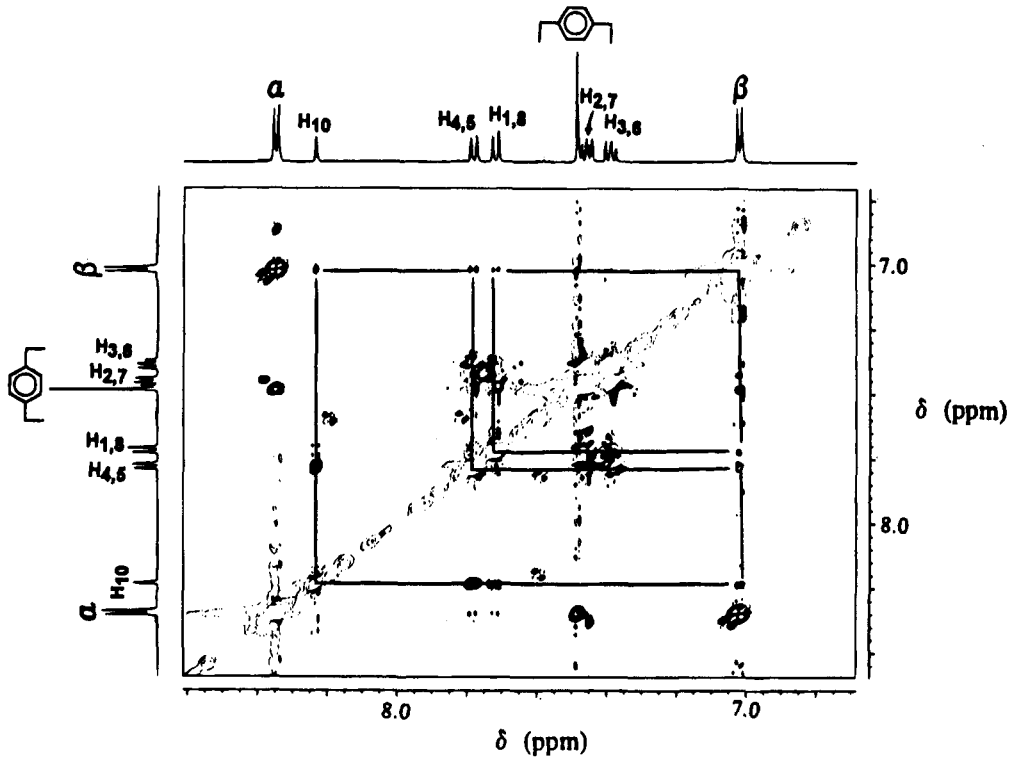

Figure 7. Partial ROESY ^{1}H NMR spectrum recorded for **1** in CD_3CN at +25 °C showing NOE effects between CH(β) protons and protons resident on the terminal anthracene subunits.

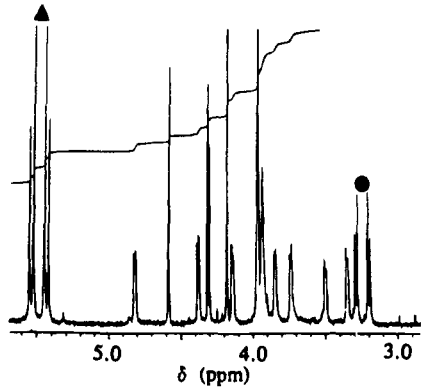

Figure 8. Partial ^{1}H NMR (500 MHz) spectra recorded for **2** in CD_3CN at +25 °C: marked are (▲) the methylene protons on the cyclophane and (●) the protons on the included dialkoxybenzene station.

However, unlike **3** at this temperature, these protons appear as a single set of resonances, presumably due to the additional degrees of freedom introduced upon incorporation of the second donor and lengthening of the string. Furthermore, the absence of a set of signals assignable to protons resident on the nonincluded phenyl ring might be taken to indicate fast oscillation of the cyclophane between the two degenerate stations.

The two major processes of interest, therefore, concern oscillation of the cyclophane along the string and π-stacking of terminal stopper and/or extra station to the exterior of the cyclophane. In order to further examine these processes, NMR spectra were recorded in acetone-d_6 at tempertures within the range 25 to −80 °C. Cooling to 15 °C caused broadening of signals attributed to protons resident on the terminal ferrocene subunits and concomitant appearance of a very broad signal at $\delta \approx 6.5$, which can be assigned to protons on the nonincluded phenyl ring. Presumably, these observations indicate a reduction in the rate at which the cyclophane oscillates along the string and an increased tendency for the ferrocene subunit to bind to the exterior of the cyclophane. Upon further cooling, coalescence temperatures[36] for protons resident on distal and proximal cyclopentadienyl rings, respectively, were determined to be 0 and +5 °C. A significant upfield shift occurs for one set of these resonances which suggests that the two ferrocene subunits become isolated in increasingly dissimilar environments as the temperature decreases. The characteristic AA′BB′ pattern of the nonincluded phenyl ring becomes evident at −20 °C, further indication that the two ends of the thread are becoming increasingly disparate.

Marked changes in the NMR spectral patterns for all signals associated with the cyclophane are observed at −15 °C. In particular, signals due to the methylene protons are split, and the doublet pattern observed at higher temperature for the CH(α) and CH(β) protons is removed due to line broadening. Around −30 °C, signals due to the CH(α) and CH(β) protons split into two doublets, although definite chemical shift values are difficult to ascertain because of spectral overlap. Lowering the temperature to −60 °C causes further broadening of signals arising from the cyclophane such that the AB pattern noted for the methylene protons collapses to a broad singlet. A similar effect is noted for the CH(α) and CH(β) protons. At this temperature, signals due to the xylyl protons are broadened to such an extent that two singlets are observed.

Additional information about the molecular architecture of [2]rotaxane **4** was obtained from NOE effects observed at −30 °C. Thus, irradiation at a frequency ($\delta = 6.38$) corresponding to protons located on the nonincluded phenyl ring gave rise to two clear NOE effects. First, saturation transfer occurs to the included benzene ring ($\delta \approx 3.75$). This finding suggests to us that the cyclophane still oscillates between the two benzene rings incorporated into the string at this temperature. Second, weak NOE effects are observed to all protons resident on the cyclophane, especially the methylene protons ($\delta \approx 6.0$). This latter finding is considered to be consistent with the nonincluded

(35) Hunter, C. A.; Sanders, J. K. M. *J. Am. Chem. Soc.* **1990**, *112*, 5525.

(36) The coalescence temperature is defined as that temperature at which the two peaks in a doublet merge into one. This value was determined by recording ^{1}H NMR spectra as a function of temperature until coalescence was attained.

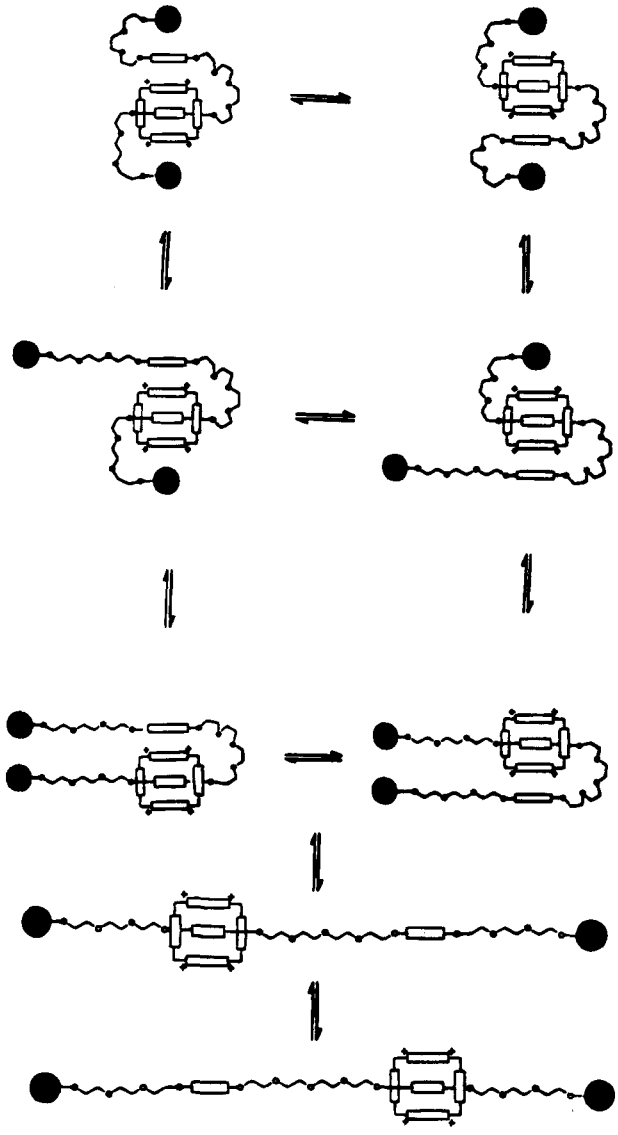

Figure 9. Major conformational exchange processes believed to occur for the two-station [2]rotaxanes. The important steps involve (i) oscillation of the cyclophane along the extended string and (ii) association between terminal stopper, unoccupied station, and cyclophane. All processes are considered to occur simultaneously.

phenyl ring being situated in close proximity to the exterior of the cyclophane. As such, the string must fold so as to facilitate π-stacking between phenyl ring and cyclophane; similar effects have been reported previously for closely-related [2]rotaxanes.[18,30,32]

The ^{1}H NMR spectrum of [2]rotaxane **5** in acetone-d_6 at 25 °C is exceedingly broad and, as a consequence, provides little useful information. Even so, the characteristic doublet patterns of the CH(α) and CH(β) protons from the 4,4′-bipyridinium subunit and the singlet for the aromatic protons of the xylyl groups comprising the cyclophane are assignable in the aromatic region. The signal for the nonincluded phenyl ring appears as a broad resonance at $\delta \approx 6.5$, which might be indicative of a slower rate of oscillation of the cyclophane along the string in **5** than in **4**. Indeed, the AB pattern of the methylene protons of the cyclophane and the AA′BB′ pattern of the nonincluded phenyl ring become clearly apparent at 0 °C, whereas these particular patterns appear only at somewhat lower temperatures for [2]rotaxane **4**. It is also apparent at 0 °C that the signal assignable to the protons on the *O*-methylene group adjacent to the carbonyl group (i.e., $\delta = 4.8$ ppm) is split into two poorly-resolved peaks.

On cooling to −30 °C, signals associated with both cyclophane and anthracene stoppers become well resolved. In particular, the signal due to the CH(α) protons of the cyclophane appears as two doublets at $\delta = 9.10$ and 8.90. This upfield shift for one of the CH(α) protons indicates that the group is being subjected to a significant shielding effect. Similar behavior is observed for the CH(β) protons and for protons on the terminal anthracene stoppers, where twin sets of resonances appear with one set being shifted upfield. As observed for [2]-rotaxane **4** further cooling causes broadening of signals associated with the cyclophane, indicating that additional conformational changes are in progress. In particular, at −80 °C signals from the CH(α) protons of the cyclophane had broadened sufficiently to give the appearance of a singlet at $\delta \approx 9.05$.

Complete assignment of all the aromatic resonances was made possible by examination of 2D COSY spectral data[37] collected at −30 °C, as shown in Figure 10. In particular, it is evident that signals associated with the cyclophane, dialkoxybenzene stations, and terminal anthracene stoppers appear as two sets of well-resolved resonances. This means that, under such conditions, oscillation of the cyclophane and conformational exchange of the string are sufficiently slow as to induce pronounced asymmetry into the molecule. The two sets of resonances for the dialkoxybenzene subunits are easily assigned to included and nonincluded moieties. Similarly, the presence of matching sets of resonances associated with the terminal anthracene stoppers can be explained in terms of their proximity to the cyclophane. For example, one singlet for the H(10) proton is shifted upfield by *ca.* 0.50 ppm with respect to the complementary singlet due to shielding by the cyclophane. There is no obvious indication, however, of π-stacking between these subunits at this temperature.

The appearance of two sets of signals observed for protons on the cyclophane, which is particularly evident for the CH(α) protons (Figure 10), could be explained in terms of two general concepts: First, the cyclophane might oscillate between two distinct environments. Second, the cyclophane itself might be rendered asymmetric. From other ^{1}H NMR spectral measurements, including NOE effects, it is known that for **5** migration of the cyclophane along the string is relatively slow at −30 °C. It seems likely, therefore, that the spectral patterns observed for the cyclophane arise from external binding to the unoccupied station. Close examination of the 2D COSY spectrum shows that the magnitude of the difference in chemical shift for the two sets of complementary resonances is significantly higher for the 4,4′-bipyridinium protons than for the xylyl protons. This could be taken to indicate close association between unoccupied station and one of the 4,4′-bipyridinium groups, which could occur *via* folding of the string. It is pertinent to note that NOE effects between unoccupied station and cyclophane are observed (see below) and that the chemical shift for the unoccupied station is located upfield by *ca.* 0.5 ppm of that of the isolated string.

Clear NOE effects were also observed for certain resonances characterized for [2]rotaxane **5** in acetone-d_6 at −30 °C. For example, irradiation into either set of CH(α) ($\delta = 9.03$ and 8.87) or CH(β) ($\delta = 7.76$ and 7.64) protons gave rise to pronounced NOE effects to the complementary set. Since it was established from 2D COSY that these two sets of CH(α) and CH(β) resonances are not mutually coupled under these conditions, the NOE results are best explained in terms of saturation transfer.[38] This could occur *via* oscillation of the cyclophane along the string or *via* alternation of the dialkoxybenzene subunit π-stacking with either side of the cyclophane (Figure 11). We were unable to detect any NOE effect involving the anthracene protons under irradiation into CH(α) or CH(β) protons at this temperature, even though chemical shift

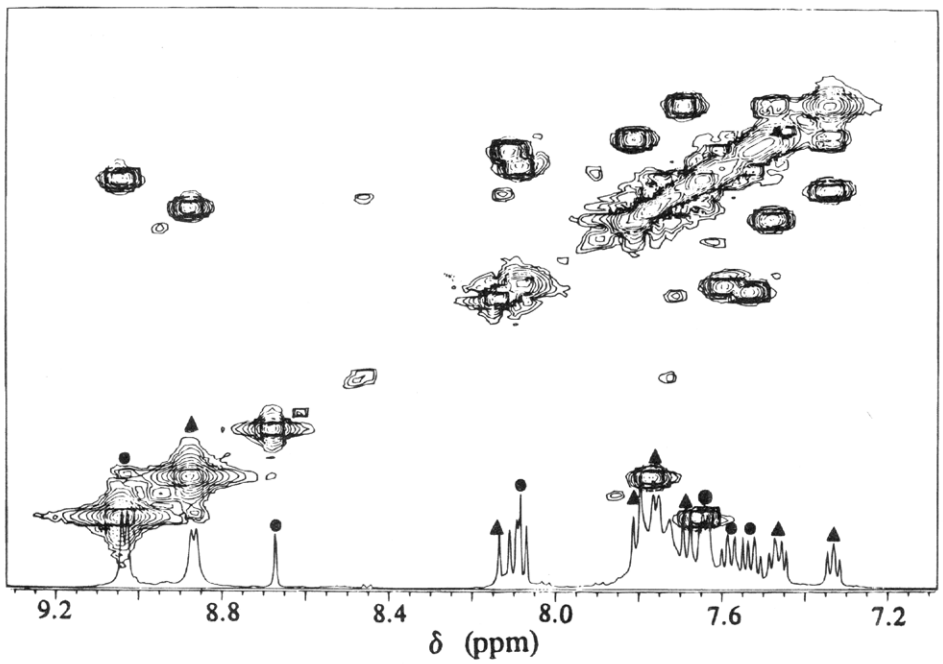

Figure 10. Partial 2D COSY spectrum recorded for **5** in acetone-d_6 at −30 °C: marked are the two sets of matching resonances with the upfield protons marked (▲) and the corresponding downfield shifted protons marked (●). Signals occurring at 9.04, 8.86, 7.79, 7.75, 7.73, and 7.64 ppm are attributed to the cyclophane and all other signals are due to the anthracene subunits.

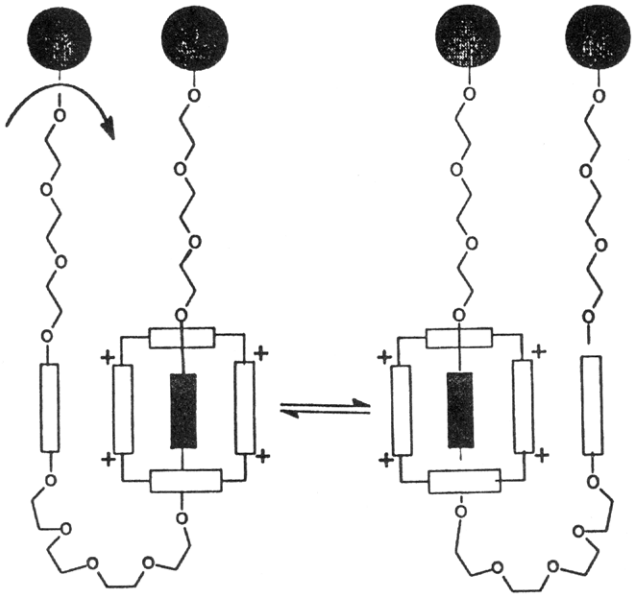

Figure 11. Pictorial representation of π-stacking between the unoccupied station and the exterior of the cyclophane for the two-station [2]rotaxanes.

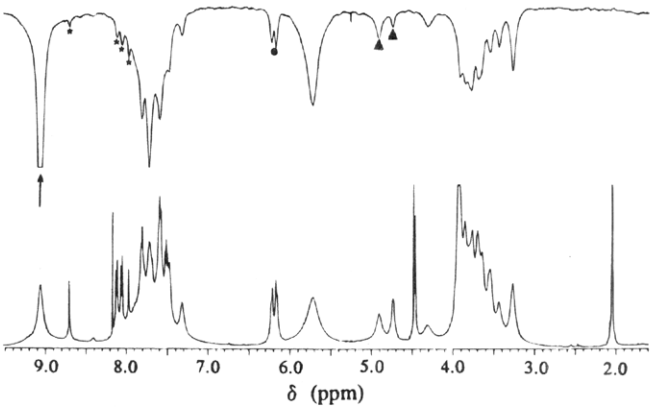

Figure 12. NOE difference spectrum recorded for **5** in acetone-d_6 at −80 °C under irradiation (δ = 9.05 ppm) into the CH(α) protons on the cyclophane. The resonances marked (*) refer to protons on the anthracene subunit, (●) refers to protons on the unoccupied station, and (▲) refers to protons adjacent to the ester group.

data suggest that both anthracene subunits are shielded. Irradiation into the nonincluded phenyl ring (δ = 6.32) shows appreciable NOE effects to protons resident on the 4,4′-bipyridinium subunit of the cyclophane. This suggests that these two subunits must come into van der Waals contact. Again, there were no apparent NOE effects to protons located on the terminal anthracene stoppers under these conditions. However, irradiation into the CH(α) protons of the cyclophane at −80 °C showed definite NOE effects to protons resident on the anthracene stoppers and to the *O*-methylene protons adjacent to the carbonyl group (Figure 12). It appears, therefore, that there is a marked decrease in entropy as the temperature is lowered; a feature that is depicted in terms of increased π-stacking in Figure 9.

Each subunit in [2]rotaxanes **4** and **5** exhibit temperature dependent ^{1}H NMR spectral patterns.[18,29,30,33] The various conformational exchanges, as depicted in Figure 9, can be loosely classified as (i) oscillation of the cyclophane along the string, (ii) association of the terminal stopper with cyclophane or unoccupied station, and (iii) π-stacking between unoccupied station and the exterior of the cyclophane. These processes occur simultaneously, each with a different activation energy and rate constant, and it is unrealistic to attempt to assign such values to individual events.

For several resonances in each [2]rotaxane, coalescence temperatures (T_c) were determined from the temperature-dependent ^{1}H NMR spectra, while the difference in chemical shift for matching pairs of resonances at very slow exchange ($\Delta\delta$) were measured at low temperature (Table 3). These values were subsequently used to calculate the exchange rate constant at the coalescence temperature (k_c)[39] and, from the Eyring equation,[40] the coalescence activation energy (ΔG_c*). A common activation energy of (13.6 ± 0.9) kcal mol^{-1} was obtained for all the resonances monitored and for both **4** and **5** (Table 3), and it should be recalled that very similar ΔG_c* values have been reported previously for related [2]rotaxanes.[18,29,30,33] This suggests that all the resonances monitored are being subjected

Table 3. Kinetic and Thermodynamic Parameters Estimated from Dynamic ^{1}H NMR Studies Made for the Two-Station [2]Rotaxanes

compd	resonance	T_c (°C)	$\Delta\delta$ (Hz)	k_c (s^{-1})	ΔG_c^* (kcal mol^{-1})
4	CH(α)	−10	17	37	13.4
	CH(β)	−10	22	50	13.3
	CH_2[a]	−5	18	40	13.7
	disFc[b]	0	144	320	12.8
	proFc[c]	+5	58	130	13.6
5	CH(α)	−5	85	190	12.8
	CH(β)	−10	44	100	12.9
	CH_2[a]	+5	28	60	14.0
	CH_2O[d]	+20	75	165	14.2

[a] Methylene protons on the cyclophane. [b] Protons on the distal ferrocene ring. [c] Protons on the proximal ferrocene ring. [d] Methylene group adjacent to the ester group.

to the same global exchange processes but it must be emphasized that, when used in this manner, the Eyring equation[41] is not sensitive to small changes in T_c. Furthermore, the apparent magnitude of the activation energy is a direct consequence of assigning a fixed value for the activationless rate constant of 4.6×10^{10} s^{-1} in the Erying equation. Calculating the exchange rate for various resonances at different temperatures, using two-site theory,[42] and applying the Arrhenius expression gave rise to activation energies that were much lower than 13.6 kcal mol^{-1} and that were markedly dependent upon the particular resonance studied.[43] In this case, however, the pre-exponential terms appeared to be unrealistically low. Finally, the rates of exchange of the two dialkoxybenzene stations at coalescence were found to be 3100 and 2900 s^{-1}, respectively, for **4** and **5**.

Summary of Structural Information. On the basis of X-ray crystallography, ^{1}H NMR, and allowing for previous work with closely-related molecular systems,[18,29] several structural features of these [2]rotaxanes can be highlighted. First, it is clear that for one-station [2]rotaxanes the cyclophane lies preferentially over the central dialkoxybenzene donor. For the corresponding two-station [2]rotaxanes, the cyclophane migrates incoherently along the string[29,33b] but prefers to reside over one of the dialkoxybenzene subunits rather than on the string itself. Second, the terminal stoppers, because of their aromatic character, closely associate with the pyridinium rings of the cyclophane.[17] This has the effect of forming "closed" conformations in which π-stacking extends throughout the molecule. For example, the various aromatic subunits in **3** align so as to position seven aromatic rings into a single π-stack. For the two-station [2]rotaxanes there is additional association between the unoccupied station and the exterior of the cyclophane. Third, the structures are dynamic, at least on the NMR time scale. This is a particular feature of the two-station [2]rotaxanes where one of the dialkoxybenzene groups must be outside the cyclophane cavity at any given time. The various conformational exchanges occur simultaneously, and it is difficult to assign rates or activation energies to specific processes.

(37) COSY is an acronym for two-dimensional correlation spectroscopy.

(38) Sanders, J. K. M.; Hunter, B. K. *Modern NMR Spectroscopy A Guide for Chemists*; Oxford University Press: Oxford, 1993.

(39) The rate of exchange at coalescence was calculated according to $k_c = (\pi/2^{1/2})\Delta\delta$ where $\Delta\delta$ is the difference in chemical shift for the two peaks under conditions of very slow exchange, see: Kost, K.; Carlson, E. H.; Raban, M. *J. Chem. Soc., Chem. Commun.* **1971**, 656.

(40) Shanan-Atidi, H.; Bar-Eli, K. H. *J. Phys. Chem.* **1970**, *74*, 961.

(41) The coalescence activation energy is estimated by comparing the observed rate at coalescence with the activationless rate derived from transition state theory. Since the latter term is high and only a narrow range of rates can be determined by NMR spectroscopy, it follows that only a relatively narrow range of activation energies can be probed by this method.

(42) Burdon, J.; Hotchkiss, J. C.; Jennings, W. B. *J. Chem. Soc., Perkin Trans. II* **1976**, 1052.

(43) Apparent activation energies calculated from Arrhenius plots ranged from 5 to 10 kcal mol^{-1}, while the activationless rates were found to vary from 5×10^4 to 5×10^7 s^{-1}.

Table 4. Photophysical Properties Measured for the Anthracene Subunits in the Anthracene-Stoppered [2]Rotaxanes and for the Corresponding Anthracene-Containing Reference Compounds in Acetonitrile Solution at 25 °C[a]

compd	ϕ_f	τ_f (ns)
anthracene	0.27	5.1
ethyl-9-anthroate	0.21	7.0
decyl-9-anthroate	0.11	5.9
15	0.05	0.50 (83%) 6.0 (17%)
1	<0.002	0.025 (92%) 1.0 (8%)
5	0.02	0.035 (45%) 0.61 (55%)

[a] Where two lifetimes are observed, the fraction of each component is given in parentheses after the value of the lifetime.

In the one-station [2]rotaxanes, the cyclophane has restricted migration along the string, because of the shortness of the string and the presence of terminal stoppers. This migration is further hindered by the molecule adopting a closed conformation in which the stoppers associate with the cyclophane. This external π-stacking is clearly apparent in the solid state and is consistent with both NMR and time-resolved fluorescence spectroscopy (see later) in fluid solution. Anthracene stacks much more readily than does ferrocene; association constants are on the order of 11.5 and 0.36, respectively, for **1** and **3**. Interestingly, in the absence of the central cyclophane, the anthracene stoppers do not form an excimer but, according to NOE studies, do associate with the dialkoxybenzene group.

Knowledge of the probable conformation in solution is of prime importance in furthering an understanding of the photochemical processes that occur upon direct excitation into the charge-transfer absorption band. Such information is also essential for the construction of photochemical devices based on these [2]rotaxanes. Before designing more elaborate [2]rotaxanes and catananes possessing different donors incorporated into the string, it is necessary to know how best to preorganize the structure for optimal photoinduced electron transfer. It is also important to realize that effective π-stacking between terminal subunits and the central cyclophane increases the synthetic yield of the final [2]rotaxane.

Fluorescence from the Terminal Anthracene Stoppers. In dilute acetonitrile solution at room temperature, ethyl 9-anthroate shows weak but well-resolved absorption bands in the near UV region. Fluorescence is readily observed,[44] the fluorescence quantum yield (Φ_f) in acetonitrile solution being 0.21, while the fluorescence lifetime (τ_f), measured by time-correlated, single-photon counting methodology, was found to be (7.0 ± 0.1) ns (Table 4). The fluorescence decay profile was well-described in terms of a single exponential. Comparable absorption and fluorescence properties were observed for decyl 9-anthroate in acetonitrile solution ($\Phi_f = 0.11$; $\tau_f = 5.9$ ns). It should be noted that the fluorescence spectra recorded for the alkyl anthroates[44] differ markedly from that of anthracene ($\Phi_f = 0.27$; $\tau_f = 5.1$ ns) (Table 4) since the fluorescence profile is essentially structureless and there is a significant Stokes shift (i.e., 5500 cm^{-1}). Such properties can be used to infer that there is a substantial geometric change upon excitation and that the fluorescent state possesses charge-transfer character. From space-filling molecular models, we conclude that steric hindrance between the carbonyl group and the adjacent *peri* hydrogen atoms keeps the carbonyl group orthogonal to the anthracene ring in the ground state. It is possible, therefore, that following light excitation the carbonyl group rotates so as to increase any charge-transfer interaction with the aromatic ring.

For precursor **15**, having a single anthroate group linked to a dialkoxybenzene subunit, the absorption spectrum remains

(44) Shon, M. S.-L.; Cowan, D.; Schmlegel, W. W. *J. Phys. Chem.* **1975**, *79*, 2087.

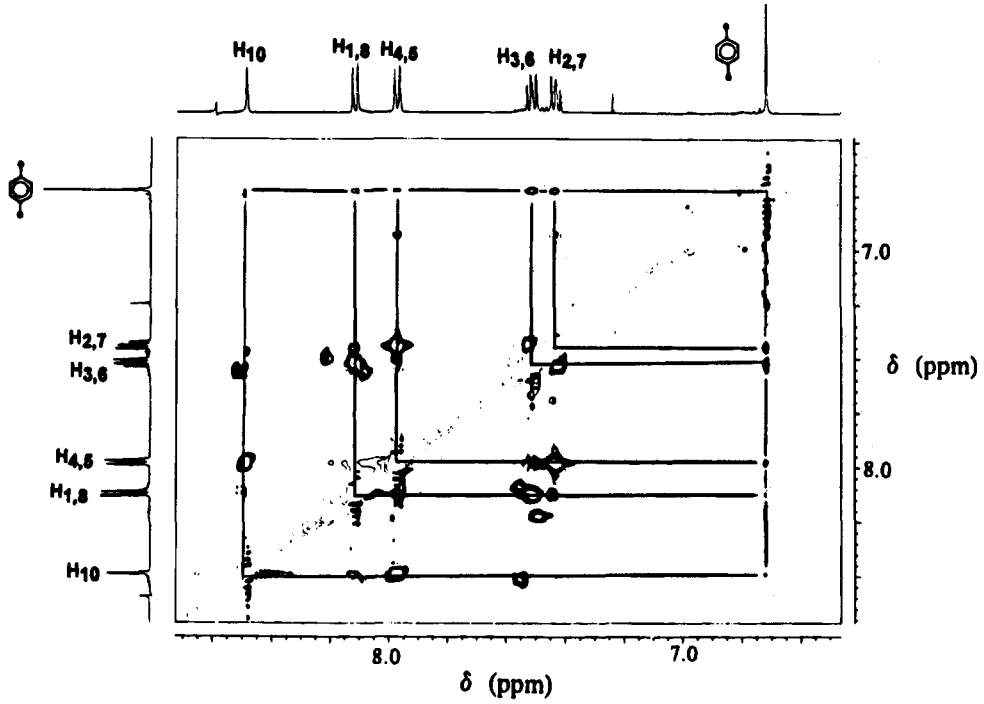

Figure 13. Partial NOESY spectrum recorded for **8** in $CDCl_3$ at +5 °C showing clear NOE effects between protons on the phenyl and anthracene rings.

similar to that observed for ethyl 9-anthroate, but fluorescence is greatly diminished (Φ_f = 0.05). The fluorescence decay profile could not be fit to a single exponential but corresponded to the sum of two-exponential components with lifetimes of (500 ± 50) ps and (6.0 ± 0.1) ns (Table 4). The shorter-lived component accounted for *ca.* 80% of the initial fluorescence intensity. The fluorescence properties of the anthracene-containing strings **8**, **10**, and **12** were similar to those reported above for **15**, and, in particular, the fluorescence decay profiles required analysis in terms of two exponentials. It should be noted that the strings containing two terminal anthracene stoppers (i.e., **8** and **12**) did not exhibit excimer fluorescence.[45]

It is unlikely that the above fluorescence quenching arises from photoinduced electron transfer from the dialkoxybenzene donor to the excited singlet state of the anthracene chromophore. On the basis of cyclic voltammetry measurements made in acetonitrile solution, the thermodynamic driving force for this electron transfer process is calculated to be *ca.* +0.43 eV.[46] Laser flash photolysis studies carried out with **8** in acetonitrile solution, for excitation with a 30-ps pulse at 355 nm, showed that the excited singlet state of the anthracene chromophore was present immediately after the laser pulse. This species decayed with a lifetime of *ca.* 500 ps, leaving a small residual signal that could be identified as the triplet excited state. Electron-transfer products, and in particular the π-radical anion of the anthracene subunit, were not apparent in the decay records. From NOE measurements made with **8** in $CDCl_3$ at 5 °C, it is apparent that the aromatic protons on the dialkoxybenzene subunit show significant NOE effects to H(1,8), H(4,5), and H(10) protons on the terminal anthracene subunit (Figure 13). This finding, taken together with the modest chemical shift differences observed between **8** and decyl 9-anthroate, is consistent with association between the aromatic subunits. This association, in turn, might force the carbonyl group to adopt a geometry

(45) It is possible that any excimer formed by diffusional encounter between the terminal anthracene subunits undergoes net electron transfer but the corresponding π-radical ions could not be detected by picosecond transient absorption spectroscopy. Furthermore, fluorescence quantum yields remained similar for compounds containing one and two anthracene moieties.

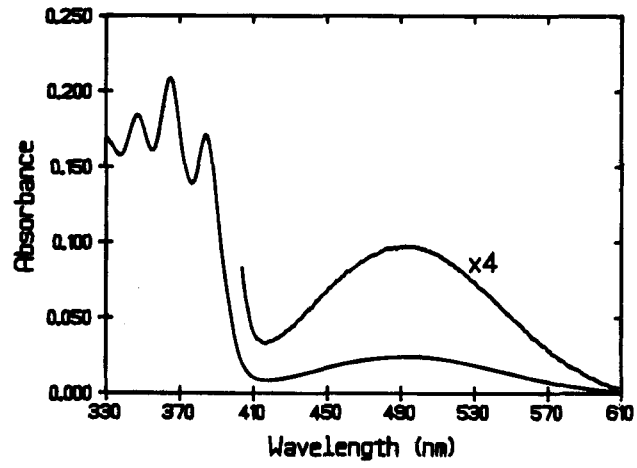

Figure 14. Absorption spectrum recorded for **1** in CH_3CN.

that is highly favorable for charge-transfer interaction with the anthracene ring. In this case, the shorter-lived component observed in the fluorescence decay profiles (i.e., that responsible for quenching) may be attributed to a "closed" conformation in which there is increased charge-transfer character in the lowest energy excited singlet state. The longer-lived species, therefore, is assigned to an "open" conformer having less charge-transfer character in the excited singlet state.

Fluorescence from the terminal anthracene stoppers in the one-station [2]rotaxane **1** was extensively quenched (Φ_f < 0.002) relative to ethyl 9-anthroate in acetonitrile solution. The absorption spectrum indicates that the $\pi-\pi^*$ transitions localized on the anthracene subunits overlap with a weak charge-transfer transition characteristic of the central donor–acceptor complex (Figure 14). Time-resolved fluorescence decay profiles recorded for **1** required analysis in terms of two exponential components. The major component, accounting for 92% of the initial fluorescence intensity, corresponded to a lifetime of (25 ± 5) ps while the minor component (i.e., 8%) had a lifetime of (1.0 ± 0.1) ns (Table 4). These two fluorescing species can be attributed to closed and open conformers in which the anthracene moiety is, respectively, adjacent to or distant from the central

cyclophane. This situation is entirely consistent with our NMR studies, while close association of the subunits is known to occur in the solid state. On the basis of the relative intensities of these two fluorescing species, the association constant for the closed conformer can be estimated as 11.5 (i.e., $\Delta G^\circ \approx -6$ kJ mol^{-1}).

Fluorescence quenching in the [2]rotaxane is attributed to electron transfer from the excited singlet state of the anthracene chromophore to one of the 4,4′-bipyridinium dications comprising the cyclophane. The Gibbs free energy change for this process, as estimated from cyclic voltammetry, is *ca.* −0.71 eV.[47] Laser flash photolysis studies, for excitation at 305 nm with a 1-ps pulse, indicated that the excited singlet state of the anthracene chromophore was present immediately after excitation. This species decayed *via* first-order kinetics, with a lifetime of (30 ± 5) ps, to leave a residual absorption that could be assigned to electron-transfer products. These latter species decayed *via* first-order kinetics with a lifetime of (140 ± 30) ps due to charge recombination ($\Delta G^\circ \approx -1.97$ eV).

Weak fluorescence ($\Phi_f \approx 0.02$) was also observed from the anthracene-stoppered, two-station [2]rotaxane **5** in acetonitrile solution (Table 4). Again, the fluorescence decay profile required analysis in terms of two-exponential components but, unlike the situation with **1**, the two components contributed almost equally to the initial fluorescence intensity. The longer lifetime, which accounted for *ca.* 55% of the initial fluorescence, was found to be (610 ± 50) ps. This value is similar to that previously assigned to an anthracene chromophore held in close proximity to a dialkoxybenzene subunit. It is, therefore, attributed to the terminal anthracene subunit that is remote from the cyclophane. To account for its relatively short lifetime, it is necessary to invoke π-stacking between anthracene and appended dialkoxybenzene subunits. The shorter lifetime, which accounts for *ca.* 45% of the initial fluorescence, was found to be (35 ± 10) ps. This value is comparable to that characterized for an anthracene chromophore held adjacent to the cyclophane subunit. We assign this species, therefore, to the terminal anthracene stopper that is closest to the cyclophane; it should be noted that according to ^{1}H NMR studies the cyclophane is frozen on the time scale of the fluorescence studies.

Charge-Transfer Absorption Spectroscopy. An unwelcome aspect of π-stacking between terminal stopper and cyclophane is that it might interfere with the primary charge-transfer complexation between cyclophane acceptor and dialkoxybenzene donor. Strong complexation between these latter subunits, which is known to occur in simpler systems,[10,13] is essential for the development of photochemical devices. Such charge-transfer interactions can be probed by absorption spectroscopy since the various charge-transfer complexes exhibit discrete absorption spectral bands. Thus, *N,N*′-dimethyl-4,4′-bipyridinium dication forms intermolecular charge-transfer complexes with 1,4-dimethoxybenzene, ethyl 9-anthroate, and ferrocene. The derived association constants (*K*), absorption maxima (λ_{max}), and molar extinction coefficients at the absorption maximum (ϵ_{max}) are compiled in Table 5. It is seen that the position of the absorption maximum depends on the oxidation potential of the donor (E_{ox}). Fitting the observed absorption spectrum to a Gaussian profile and applying Hush theory[48] allows derivation of the magnitude of electronic coupling (*H*) between the reactants in the charge-transfer complex.

$$H = 0.0206[\epsilon_{max} E_{op} \Delta\nu_{1/2}]^{1/2}/d \quad (1)$$

Here, E_{op} is the energy (in cm^{-1}) of the absorption maximum, $\Delta\nu_{1/2}$ is the half-width of the Gaussian-shaped absorption band (in cm^{-1}), and *d* is the distance between the partners in the complex (*d* = 3.4 Å). The relevant values are collected in Table 5, and it can be seen that, apart from the respective absorption maxima, the properties are relatively insensitive to the nature of the donor. In particular, the association constants are exceedingly small.

Table 5. Properties of the Charge-Transfer Absorption Bands Recorded in CH_3CN for Various Intermolecular and Cyclophane-Derived Systems

compd	*K* (M^{-1})	λ_{max} (nm)	ϵ_{max} (M^{-1} cm^{-1})	*H* (cm^{-1})	E_{ox} (V vs SCE)	E_{red} (V vs SCE)
PQ/DMB[a]	0.5	406	670	1740	1.41	−0.79
PQ/Fc[b]	0.2	600	550	1230	0.46	−0.79
PQ/Et ant[c]	0.1	375	440	1470	1.63	−0.79
1		486	560	1410	1.37	−0.34
2		480	600	1530	1.43	−0.36
3		478	350	1270	1.40	−0.53
4		475	1000	2140	1.38	−0.40
5		485	990	1860	1.37	−0.34

[a] Intermolecular charge-transfer complex formed between *N,N*′-dimethyl-4,4′-bipyridinium and 1,4-dimethoxybenzene. [b] Intermolecular charge-transfer complex formed between *N,N*′-dimethyl-4,4′-bipyridinium and ferrocene. [c] Intermolecular charge-transfer complex formed between *N,N*′-dimethyl-4,4′-bipyridinium and ethyl-9-anthroate.

Neither ferrocene nor ethyl 9-anthroate are accommodated inside the central cavity of the cyclophane, but they form charge-transfer complexes by association with its exterior. In such cases, the properties of the resultant complexes are similar to those reported in Table 5. 1,4-Dimethoxybenzene, however, readily includes into the cavity of the cyclophane[10] and, thereby, forms a more stable charge-transfer complex ($K = 18$ M^{-1}) in acetonitrile solution. The absorption maximum ($\lambda_{max} = 420$ nm), molar extinction coefficient ($\epsilon_{max} = 420$ M^{-1} cm^{-1}), and electronic coupling matrix element ($H = 1300$ cm^{-1}) for the cyclophane-derived complex remain comparable to the values found for complexation with *N,N*′-dimethyl-4,4′-bipyridinium dication (Table 5). It should be noted, however, that the absorption maximum is red-shifted by *ca.* 15 nm relative to the non-cyclophane system. Incorporating 1,4-dimethoxybenzene and 4,4′-bipyridinium dication subunits into a macrocyclic ring[34] gives rise to a face-to-face charge-transfer complex exhibiting an absorption maximum at 397 nm in acetonitrile solution ($\epsilon_{max} = 130$ M^{-1} cm^{-1}; $H = 900$ cm^{-1}). Thus, the 15 nm red-shift appears to be characteristic of including the donor into the cyclophane cavity.

Charge-transfer absorption bands are clearly apparent for [2]-rotaxanes **1**−**5**, and the spectral properties are provided in Table 5. Inspection of the data indicates that there are significant differences in absorption maxima noted for the various [2]-rotaxanes according to the nature of the terminal stoppers. For the corresponding [2]rotaxane with triisopropylsilyl groups as terminal stoppers,[49] the charge-transfer absorption maximum in acetonitrile solution occurs at 470 nm. Thus, the anthracene-stoppered [2]rotaxanes **1** and **5** exhibit red-shifts of *ca.* 16 nm relative to the nonaromatic-stoppered system while the ferrocene-stoppered [2]rotaxanes **3** and **4** show blue shifts of *ca.*

(46) Calculated according to $\Delta G^\circ = -[E_{red} - E_{ox} + E_{ex}]$ where E_{red} (= −1.70 V vs SCE) and E_{ox} (=1.41 V vs SCE) refer, respectively, to the one-electron redox potentials for reduction of the anthracene chromophore and for oxidation of the terminal dialkoxybenzene subunit. The term E_{ex} (=2.68 eV) is the excitation energy of the chromophore.

(47) Calculated according to $\Delta G^\circ = -[E_{red} - E_{ox} + E_{ex}]$ where E_{red} (= −0.34 V vs SCE) and E_{ox} (=1.63 V vs SCE) refer, respectively, to the one-electron redox potentials for reduction of the cyclophane acceptor and for oxidation of the terminal anthracene subunit. The term E_{ex} (=2.68 eV) is the excitation energy of the chromophore.

(48) Hush, N. S. *Prog. Inorg. Chem.* **1967**, *8*, 391.

(49) Stoddart, J. F. *Host−Guest Molecular Interactions: from Chemistry to Biology*; Ciba Foundation Symposium 158: Wiley: Chicester, 1991; p 5.

3 nm. Interestingly, the charge-transfer absorption maximum for the asymmetric [2]rotaxane **2** falls between those noted for **1** and **3**. It should be emphasized, however, that the apparent absorption maxima for the ferrocene-containing [2]rotaxanes appear at lower energy because of overlap with an absorption band associated with the ferrocene subunit ($\lambda_{max} \approx 440$ nm). Subtracting the contribution of the ferrocene absorption transition, as observed for the individual strings, gave estimates for the charge-transfer absorption maxima of 480, 478, and 475 nm, respectively, for **2**, **3**, and **4**. The magnitude of the apparent red-shifts, measured relative to the nonaromatic-stoppered [2]-rotaxane, correlates with the stated affinity of the terminal stopper to π-stack with the cyclophane and it is pertinent to recall that comparable shifts are observed for both one- and two-station [2]rotaxanes.

The optical absorption maximum of a charge-transfer band depends[7] upon the free energy change for charge transfer, a term representing any additional electronic energy associated with excitation (including the total reorganization energy that accompanies charge transfer), and a term for the resonance integral. The latter term allows for changes in orientation of the donor and acceptor subunits. In turn, the free energy change is related to the difference between the one-electron reduction potential of the cyclophane (E_{red}) and the one-electron oxidation potential of the donor (E_{ox}), and to a term describing any change in electrostatic potential. Cyclic voltammetric measurements made for [2]rotaxanes **1**−**5** indicated that the redox potential for one-electron reduction of the cyclophane acceptor was sensitive to the nature of the terminal stopper (Table 5). This suggests to us that differences in the maxima of the charge-transfer absorption bands are related to changes in the thermodynamic driving force for charge transfer, although it is likely that small changes also occur in the reorganization energy. The charge-transfer absorption transition moment lies perpendicular to the aromatic π-systems,[50] and, therefore, small changes in orientation are manifest in significant changes in molar extinction coefficient (Table 5).

Direct Excitation into the Charge-Transfer Absorption Band. The photochemistry that ensues upon excitation into the charge-transfer absorption band of intermolecular electron donor−acceptor complexes,[9] cyclophane-derived charge-transfer complexes,[10] and covalently-linked, face-to-face, charge-transfer complexes[34] containing relevant redox-active subunits has been described previously. Also, the photochemistry of [2]rotaxane **3** has been reported.[15] The general behavior is similar in each case and can be summarized as follows: Irradiation into the charge-transfer absorption band generates an excited state in which charge has been transferred from the dialkoxybenzene donor to the nearby 4,4′-bipyridinium dication acceptor. Because of the increased electrostatic repulsion between the subunits in the excited state there will be some structural rearrangement of the initial Franck−Condon state, subject to constraints imposed by the molecular architecture. The relaxed state may be considered to be an intimate radical ion pair and undergoes rapid charge recombination to restore the ground-state species. In certain cases where the rate of charge recombination is sufficiently slow and the structure is sufficiently flexible, the radical ion pair can dissociate into solvent-separated radical ions. For [2]rotaxane **3** there is the additional feature that the dialkoxybenzene π-radical cation, comprising part of the radical ion pair, can oxidize the terminal ferrocene stopper and, thereby, facilitate spatial separation of the charges.[15] We now compare the photochemistry of the new [2]rotaxanes with that evaluated previously for [2]rotaxane **3**.

(50) Borkent, J. H.; Verhoeven, J. W.; de Boer, Th. J. *Chem. Phys. Lett.* **1976**, *42*, 50.

Table 6. Lifetimes of the Primary Radical Ion Pair (τ_{rip}) Measured for the Various [2]Rotaxanes in Acetonitrile Solution at 25 °C and Lifetimes (τ_{cts}) and Quantum Yields (ϕ_{cts}) for the Spatially-Separated Charge-Transfer State Formed for the Ferrocene-Stoppered [2]Rotaxanes

[2]rotaxane	τ_{rip} (ps)	τ_{cts} (ns)	ϕ_{cts}
1	14		
2	20	480	0.10
3	30	555	0.25
4	27	1100	0.08
5	17		

Excitation of [2]rotaxane **1** in acetonitrile solution at 25 °C with a subpicosecond laser pulse at 440 nm resulted in formation of the thermally-relaxed, intimate radical ion-pair (RIP) within a few ps. This species results from transfer of charge from the included dialkoxybenzene donor to the cyclophane acceptor and subsequent structural relaxation. The RIP exhibits a characteristic transient absorption spectrum (Figure 15a), as reported previously for related systems.[10,15] Decay of the RIP occurs *via* first-order kinetics with a lifetime (τ_{rip}) of (14 ± 4) ps (Table 6) and restores the ground-state system (Figure 15b). In this case, there is no secondary electron transfer involving the terminal anthracene stoppers since this process is thermodynamically unfavorable ($\Delta G° \approx 0.26$ eV).[51] Similar behavior was found for the two-station [2]rotaxane **5**, where the lifetime of the RIP was measured as (17 ± 5) ps (Table 6). It is apparent, therefore, that migration of the cyclophane along the string cannot compete with charge recombination. In fact, the temperature-dependent NMR studies have been interpreted in terms of relatively slow oscillation of the cyclophane about the dialkoxybenzene station. Estimating an upper limit for the diffusion coefficient (D) of the cyclophane subunit in these [2]-rotaxanes as being *ca.* 10^{-6} cm^2 s^{-1} the maximum translational distance (d) expected for the cyclophane within a 20 ps time period ($d = [2Dt]^{1/2}$) is calculated to be less than 1 Å. There is, therefore, no dissociation of the RIP within its short lifetime, and the photonic energy is simply converted into heat (Chart 1). Such systems possess no obvious application as photochemical devices.

Similar experiments made with [2]rotaxane **2** in acetonitrile solution allowed determination of the lifetime of the RIP as being (20 ± 5) ps (Table 6). Here, rapid restoration of the ground state was incomplete, and about 10% of the initial signal persisted on much longer time scales (Figure 15c). Subsequent investigation of the kinetic behavior with inferior time resolution indicated that this residual signal decayed *via* first-order kinetics with a lifetime of (480 ± 30) ns (Table 6). Based upon results obtained previously with **3**, the long-lived signal is attributed to a redox pair in which the oxidizing equivalent has been transferred from the included dialkoxybenzene π-radical cation to the terminal ferrocene stopper ($\Delta G° \approx -1.01$ eV).[15] Reverse charge transfer between the ferrocenium cation and the one-electron reduced cyclophane ($\Delta G° \approx -0.78$ eV) restores the ground-state system. Similar behavior was observed with the asymmetric two-station [2]rotaxane **4** where the lifetime of the RIP was found to be (27 ± 5) ps (Table 6). In this latter case, the lifetime of the residual signal (τ_{cts}), which was formed with a quantum yield (ϕ_{cts}) of *ca.* 8% yield, was extended to (1.1 ± 0.2) μs (Table 6).

The derived rates of primary charge recombination for the various [2]rotaxanes remain comparable; the lifetime of the RIPs varies from 14 ps for **1** to 30 ps for **3**. Examination of the

(51) Calculated according to $\Delta G° = [E_{stop} - E_{ox}]$ where E_{ox} (=1.37 V vs SCE) and E_{stop} (= 1.63 V vs SCE) refer, respectively, to the one-electron redox potentials for oxidation of the included dialkoxybenzene subunit and for the anthracene stopper.

Chart 1

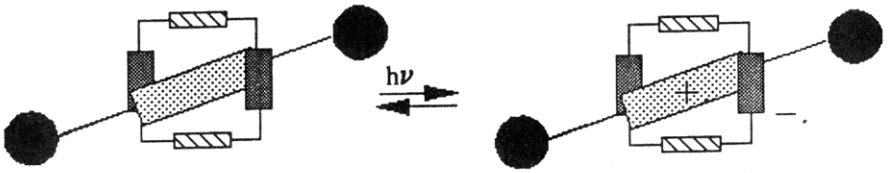

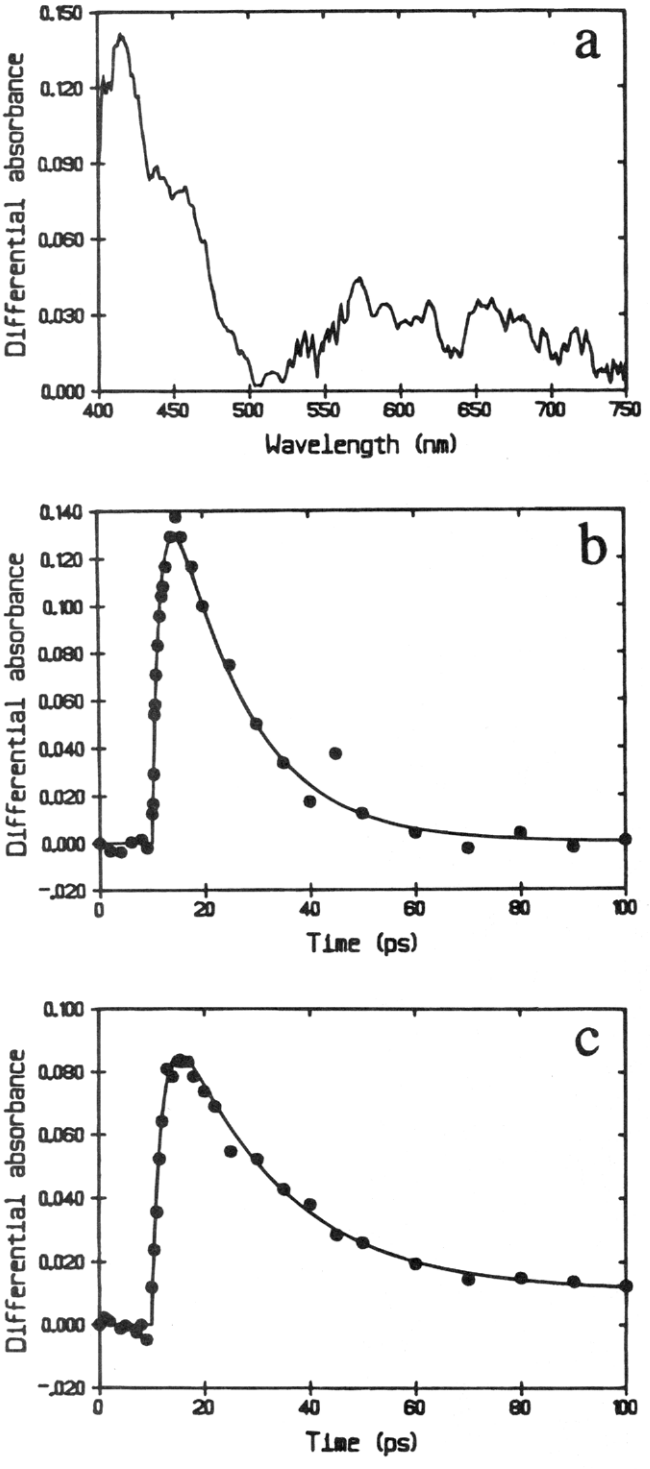

Figure 15. (a) Transient differential absorption spectrum recorded 2 ps after excitation of **1** in CH_3CN with a sub-ps laser pulse at 440 nm. (b) Kinetic profile recorded at 400 nm for the above experiment. (c) Kinetic profile recorded at 400 nm for **2** after irradiation under identical conditions.

kinetic data indicates that the lifetime of the RIP increases with increasing energy of the charge-transfer absorption band (as measured from the absorption maximum). This effect was observed previously for nonstoppered, cyclophane-derived systems[10] and explained in terms of a simple energy-gap law. Thus, in cases where the energy content of the RIP ($-\Delta G°$) greatly exceeds the reorganization energy that accompanies charge recombination the lifetime of the RIP is controlled by the rate of energy dissipation among certain vibrational modes. This situation is analogous to nonradiative deactivation of excited states and can be explained quantitatively in terms of the Englman–Jortner theory.[52] There is ever-growing indications[34] that this theory also explains charge recombination within intimate RIPs, and, at least in qualitative terms, it accounts for our observations regarding the lifetimes of the RIPs formed from the various [2]rotaxanes. As a consequence, increasing the amount of energy that the RIP must dissipate *via* vibrational transitions ($E_{op} = hc/\lambda_{max}$) results in an inevitable increase in lifetime of the RIP. Binding of the terminal stopper, especially anthracene, to the exterior of the cyclophane has the effect of lowering the energy of the RIP (Table 5), and this effect is manifest in a slight decrease in the lifetime of the RIP (Table 6).

In the ferrocene-containing [2]rotaxanes, oxidation of a terminal ferrocene subunit by the included dialkoxybenzene π-radical cation competes with charge recombination within the RIP (Chart 2). The rate constant for this secondary oxidation process ($k = \phi_{cts}/\tau_{rip}$) is *ca.* 5×10^9 s^{-1} ($\Delta G° = -1.0$ eV) for the various [2]rotaxanes. This process is slow relative to charge recombination so that the quantum yield for formation of spatially-remote charge-transfer products (ϕ_{cts}) is kept low (Table 6). The rate of oxidation of the ferrocene subunit, however, appears to be far too high for electron transfer along an extended string[53] or for a through-space process between widely-spaced partners.[54] Instead, it is more likely that secondary electron transfer occurs only within a conformation in which a ferrocene subunit is closely-associated with the exterior of the cyclophane. Such conformations have been observed in the solid state X-ray structure and are consistent with the solution phase NMR studies. This π-stacking between terminal ferrocene and one of the 4,4′-bipyridinium dicationic subunits of the cyclophane not only brings the reactants into fairly close proximity but also facilitates a superexchange mechanism[55] for the secondary electron-transfer event by making use of orbitals on the intervening aromatic moiety. In this latter case, electron transfer would proceed through LUMO or HOMO orbitals localized on the 4,4′-bipyridinium dication without this species appearing as a real redox intermediate. On the basis of the association constant for exterior binding of ferrocene being *ca.* 0.36, as determined from the NMR studies, the rate constant for oxidation of a terminal ferrocene subunit in the various [2]rotaxanes must be *ca.* 1.5×10^{10} s^{-1}. Within this interpretation, it is clear that π-stacking between terminal stopper and cyclophane, which is permitted by the use of a highly flexible string, plays a critical role in the overall redox chemistry. In fact, it might be argued that it is only because of superexchange through the orbitals of the bridging cyclophane that secondary

(52) Englman, R.; Jortner, J. *Mol. Phys.* **1970**, *18*, 145.
(53) Paddon-Row, M. N. *Acc. Chem. Res.* **1994**, *27*, 18.
(54) Miller, J. R.; Beitz, J. V. *J. Chem. Phys.* **1981**, *74*, 6746.
(55) (a) McConnell, H. M. *J. Chem. Phys.* **1961**, *35*, 508. (b) Hoffmann, R. *Acc. Chem. Res.* **1982**, *15*, 245.

Chart 2

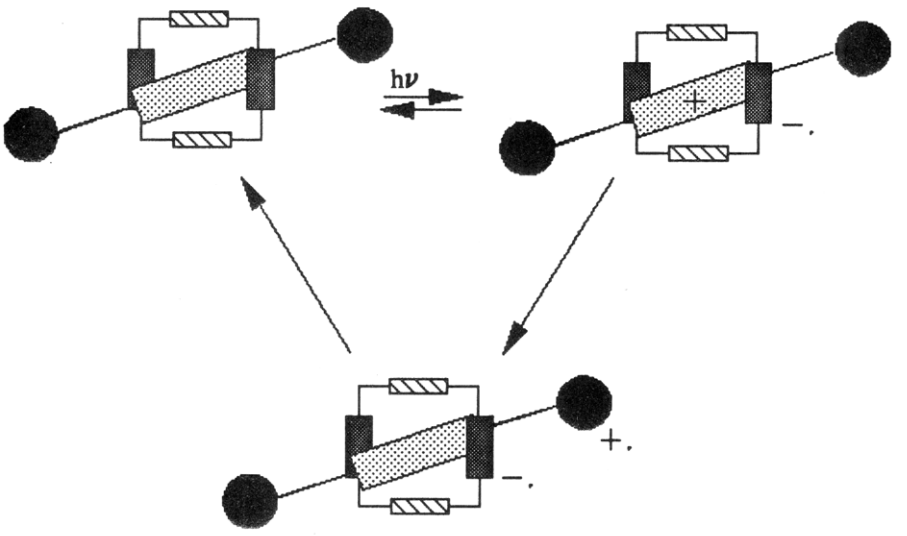

electron transfer can compete with rapid charge recombination within the RIP. Improved photochemical devices designed along these lines, therefore, will need to increase the level of π-stacking between the relevant subunits.

Subsequent to secondary electron transfer, the resultant ferricinium cation will be repelled by the positively-charged, reduced cyclophane, Thus π-stacking between these subunits will be broken, and it is likely that the string will adopt a more extended conformation that minimizes electrostatic repulsion between ferricinium and cyclophane cations. This situation, taken together with coherent migration of the cyclophane along the string in the opposite direction, since there is no longer strong affinity for the dialkoxybenzene donor within the cavity, provides for spatial separation of the charges. Indeed, the lifetime of the spatially-remote, charge-separated state (τ_{cts}) observed for the two-station [2]rotaxane is significantly longer than those observed for the corresponding one-station analogues (Table 6). This might be because of an increased separation between the reactants in the two-station [2]rotaxane, favored by the longer string. The NMR studies, however, indicate that exchange of the two dialkoxybenzene stations in **4** occurs on a much longer time scale than is needed for reverse electron transfer between ferricinium and reduced cyclophane. It is unlikely, therefore, that the cyclophane moves to the second station before reverse electron transfer takes place. This reverse electron-transfer step leads to restoration of the ground-state system (Chart 2) and, from the insensitivity of the rate constant to the intensity of the excitation pulse, must be an intramolecular process. In the absence of superexchange with orbitals localized on a bridging aromatic residue, it is reasonable to expect that reverse electron transfer involves diffusional encounter between the subunits, brought about by motion of the string. In such a case, the rate of reverse electron transfer might be controlled, in part, by the flexibility of the string.

[2]Rotaxane **2**, unlike **3** and **4**, permits directionality of secondary electron transfer because of its inherent asymmetry. The yield of separated electron-transfer products, which is about 10% for the two-station ferrocene-containing [2]rotaxanes and about 25% for the corresponding one-station analogue, is far too low for contemplation of a practical application for such systems. Furthermore, it seems appropriate to anchor one end of the thread to a macroscopic or microheterogeneous support in order to achieve genuine vectorial motion for an array of molecules. Improvements in both yield and lifetime of the separated redox products may be addressed by synthetic means, and, in particular, it should be possible to replace ferrocene with a more avid π-stacking donor. One major disappointment of the present system, which is not so easily overcome, concerns the very rapid charge recombination that occurs within the intimate radical ion pair. This situation is further exacerbated by the observation that the rate of charge recombination increases as the energy of the charge-transfer absorption band decreases. This latter finding makes it difficult to design new systems that absorb in the visible region where it is easier to selectively excite with a short laser pulse. To a limited degree, effective π-stacking between terminal stopper and cyclophane offsets the consequences of rapid charge recombination, and it will be interesting to see how efficaciously a well-designed system can be made to perform.

Acknowledgment. We thank the N.I.H. (GM 48150) for financial support of this work. The CFKR is supported by the University of Texas at Austin.

Supplementary Material Available: Tables of positional and thermal parameters, bond lengths, angles and torsional angles and figures (44 pages); lists of observed and calculated structure factors (34 pages). This material is contained in many libraries on microfiche, immediately follows this article in the microfilm version of the journal, can be ordered from the ACS, and can be downloaded from the Internet; see any current masthead page for ordering information and Internet access instructions.

JA942996H